THE UNIVERSITY OF MICHIGAN
COLLEGE OF ENGINEERING
Department of Aerospace Engineering
High Altitude Engineering Laboratory

Scientific Report

ANTENNA ADMITTANCE IN AN IONOSPHERIC-TYPE PLASMA

E. K. Miller and H. F. Schulte, Jr.

ORA Project 05627

under contract with:

NATIONAL AERONAUTICS AND SPACE ADMINISTRATION
CONTRACT NO. NASr-54(05)
WASHINGTON, D. C.

Prepared for presentation at the Nato Advanced Study Institute on Plasma Waves in Space and the Laboratory, Roros, Norway.

administered through:

OFFICE OF RESEARCH ADMINISTRATION ANN ARBOR

April 1968

Acknowledgement

The authors are pleased to acknowledge the contributions of Mr. J. W. Kuiper in several areas of this investigation.

The work was sponsored by the National Aeronautics and Space Administration, Contract No. NASr-54(05).

TABLE OF CONTENTS

List of Figures

List of Figures (Continued)

Page

ANTENNA ADMITTANCE IN AN IONOSPHERIC-TYPE PLASMA*

E. K. Miller [1] and H. F. Schulte, Jr. [2]

Abstract

An analysis of a plasma-immersed antenna, undertaken in support of an experimental program of ionospheric measurements with emphasis on the electron density, is discussed. Some numerical results for the admittance of an infinite cylindrical antenna in an ionospheric-type compressible magento-plasma show that for frequencies on the order of 1.5 to 2 times the electron cyclotron frequency (f_h), the infinite antenna admittance is relatively unaffected by the plasma compressibility and ion sheath. Consequently, the use of a finite antenna theory which neglects the plasma compressibility and sheath, such as Balmain's[3] quasistatic formula, appears to provide a reasonable first-order approximation for the impedance of an antenna in the ionosphere.

A comparison of some experimental impedance results obtained from a rocket-borne antenna experiment with values calculated from Balmain's[3] theory provides evidence of this, with good agreement being obtained between the theoretical and experimental impedance values for frequencies on the order of 2 f_h and higher. The infinite antenna impedance is found to be qualitatively in agreement with the experimental results, in particular in shifting an impedance minimum upward in frequency from f_h due to a sheath. The application of Balmain's theory to obtain the electron plasma frequency from the experimental results is discussed.

*Work sponsored by NASA Contract No. NASr-54(05).

1. Formerly with the High Altitude Engineering Laboratory, University of Michigan, now with MBAssociates, P. O. Box 196, San Ramon, Calif. 94583.

2. High Altitude Engineering Laboratory, Dept. of Aerospace Engineering, University of Michigan, Ann Arbor, Michigan 48105.

3. K. G. Balmain, The Impedance of a Short Dipole Antenna in a Magneto-plasma, IEEE Trans. AP-12, No. 5, 1964.

I. Introduction

The influence of a medium such as the ionospheric plasma upon the behavior of an antenna immersed in it is manifested by a change in the antenna impedance from its free-space value. This change may be detrimental to the use of the antenna in a communications system, but can on the other hand be used to advantage to determine various properties of the ambient ionosphere. In either case, it is obviously necessary to be able to predict as well as possible the perturbation in antenna impedance caused by the ionosphere, in the former case to optimize the antenna's performance for communication purposes, while in the latter to properly interpret the impedance results for diagnostic applications. Our interest in this problem is in connection with the use of a rocket or satellite-borne antenna as a diagnostic tool in the ionosphere.

An antenna in the ionosphere may be influenced by many factors, among which are acoustical and sheath effects which arise from the non-zero plasma temperature, and the plasma anisotropy which results from the ionospheric magnetic field. Successful application of an antenna as a diagnostic tool requires that the nature and relative importance of the roles played by each of these phonomena in determining the antenna impedance be well understood. It is this goal that has provided the motivation for the investigation to be discussed here, which was begun in support of an experimental program of ionospheric measurements with particular emphasis on the electron density.

The antenna geometry chosen for the study is that of an infinite, cylindrical dipole driven at a circumferential gap of non-zero thickness; a geometry which allows a rigorous boundary-value problem approach to be used while including in the analysis the most relevant aspects of the physics involved and at the same time describing the exciting source in a physically more credible way than the assumed current distribution often used in compressible plasma

problems. In addition, the possibility of obtaining numerical results for an interesting and realistic range of plasma parameter values, including a non-zero electron collision frequency, appeared much greater for the infinite cylindrical geometry than for finite geometries such as the biconical or prolate spheroidal, which while more realistic as far as representing a real antenna are concerned, present prohibitive analytical and numerical difficulties for the compressible, anisotropic plasma. Also, it was anticipated that the infinite antenna currents may be used to learn something of the finite antenna current, since the finite antenna may be thought of as a truncated, infinite system having multiply relfected current waves of the type propagating on the infinite antenna. Finally, it appears reasonable to expect that the medium influence of the plasma on the infinite antenna may be qualitatively similar to that expected for the finite antenna, so that the infinite antenna admittance can provide some insight into the finite antenna admittance perturbation caused by the plasma.

The actual non uniform ion sheath which forms about a body at floating potential in a warm plasma is approximated by two sheath models in the study, which we denote for obvious reasons as the vacuum sheath and inhomogeneous sheath models. Both sheath models take the sheath to be a concentric layer of finite thickness which separates the antenna from the external uniform plasma; the vacuum sheath consisting of a free-space region, while the inhomogeneous sheath takes into account the actual plasma non-uniformity in the sheath.

In the case of the compressible anisotropic plasma (in this study the static magnetic field is parallel to the antenna axis) the antenna can radiate three types of waves in the plasma medium. Two of these are basically electromagnetic (EM) in nature, while the third is basically an acoustical type wave

which we refer to as the electrokinetic (EK) wave. When the plasma is anisotropic but incompressible, only two EM waves are radiated. For the isotropic plasma a single EM wave is produced for the incompressible case, and an EM wave and EK wave may be radiated for the compressible plasma.

Coupling of the EM and EK waves may be brought about in several ways. In the discussion to follow, this consideration is restricted to boundary coupling, which may occur at a sharp plasma discontinuity, inhomogeneity coupling which results from more gradual density gradients in the plasma, and magnetic field coupling which is produced by the plasma anisotropy. The physical regions in which the various types of coupling occur are near the antenna for the boundary and inhomogeneity coupling, while the magnetic field coupling takes place throughout the volume of the plasma.

Results will be presented which demonstrate the influence of the sheath, plasma compressibility and plasma anisotropy on the infinite antenna admittance, and from which it is hoped realistic inferences may be made concerning the behavior of a finite antenna in the ionosphere. The theoretical results to be presented will be shown to be in good qualitative agreement with an extensive amount of swept-frequency impedance data obtained from a rocket-borne dipole antenna. The infinite antenna admittance calculations are also found to be substantially in agreement with calculations based on Balmain's (1964) quasistatic theory with the results of both calculations providing insight into the interpretation of the experimental measurements.

II. Theoretical Approach.

IIa. Formulation.

The fields in the plasma are obtained from the linearized fluid equations for the electrons (ion motion is neglected) together with Maxwell's equations, and may be written for an $e^{i\omega t}$ time dependence and a uniform plasma medium as

$$\nabla x \underline{E} = -i\omega\mu_o \underline{H} , \tag{1}$$

$$\nabla x \underline{H} = i\omega\epsilon_o \underline{E} - qN_o \underline{V} , \tag{2}$$

$$i\omega U\underline{V} = -\frac{q}{m}\underline{E} - \frac{v_r^2}{N_o}\nabla N - \frac{q}{m} B_o \underline{V} x \hat{z} , \tag{3}$$

$$I\omega N + N_o \nabla \cdot \underline{V} = 0, \tag{4}$$

where $\underline{E}$ and $\underline{H}$ are the time-varying electric and magnetic fields, -q, m, ν, and v_r are the electron charge, mass, collision frequency and thermal velocity, N_o and N are the static and dynamic or time-varying electron number densities, and B_o is the static magnetic field. The permeability and permittivity of free-space are denoted by ϵ_o and μ_o respectively, while

$$U = 1 + \nu/i\omega.$$

The static and dynamic electron pressures, P_o and P are assumed related to be to the electron number density by

$$P_o = kTN_o,$$

and

$$P = \gamma kTN,$$

with k Boltzmann's constant, T the electron temperature, and γ the ratio of specific heats for the electron gas. Following Cohen (1962), we set $\gamma = 3$ for assumed one dimensional, adiabatic compression, and

$$mv_r^2 = 3kT.$$

The antenna is assumed to consist of a perfectly conducting, solid cylinder of radius c located with its axis coincident with the z-axis of a cylindrical (ρ, φ, z) coordinate system, and to be cut by a gap of thickness δ centered at z = 0 which separates the two halves of the antenna. Assuming the exciting voltage to be independent of φ, and since the static magnetic field has a z-component only, then azimuthal symmetry obtains and $\frac{\partial}{\partial \varphi} = 0$ so that (1) through (4) contain derivatives with respect to ρ and z only. After a Fourier transform with respect to z,

$$\underline{E}(\rho, z) = \frac{1}{2\pi} \int_{-\infty}^{\infty} e^{i\beta z}\, \underline{e}(\rho, \beta)\, d\beta \quad ,$$

$$\underline{e}(\rho, \beta) = \int_{-\infty}^{\infty} e^{-i\beta z}\, \underline{E}(\rho, z)\, dz \quad ,$$

we obtain

$$\nabla_\beta \times \underline{e} = -i\omega\mu_o \underline{h} \quad , \tag{5}$$

$$\nabla_\beta \times \underline{h} = i\omega \epsilon_o (\underline{\underline{\epsilon}} \cdot \underline{e} - \underline{\underline{k}} \cdot \nabla_\beta n) \quad , \tag{6}$$

where ∇_β is the operator in ρ, φ, z space with $\hat{z} \frac{\partial}{\partial z}$ replaced by $i\beta\hat{z}$. Also

$$\underline{\underline{\epsilon}} = \begin{bmatrix} \epsilon_1 & -\epsilon' & 0 \\ \epsilon' & \epsilon_1 & 0 \\ 0 & 0 & \epsilon_3 \end{bmatrix} \quad , \tag{7a}$$

$$\underline{\underline{k}} = \begin{bmatrix} k_1 & 0 & 0 \\ k' & 0 & 0 \\ 0 & 0 & k_3 \end{bmatrix} \quad , \tag{8a}$$

and

$$\epsilon_1 = 1 - \frac{N^2 U}{U^2 - H^2} \quad , \tag{7b}$$

$$\epsilon' = -i \frac{N^2 H}{U^2 - H^2} \quad , \tag{7c}$$

$$\epsilon_3 = 1 - \frac{N^2}{U} \quad , \tag{7d}$$

$$k_1 = \frac{q v_r^{\,2} U}{\epsilon_o \omega^2 (U^2 - H^2)} \quad , \tag{8b}$$

$$k' = -i \frac{q v_r^{\,2} H}{\epsilon_o \omega^2 (U^2 - H^2)} = -iH/U \cdot k_1 \quad , \tag{8c}$$

$$k_3 = \frac{q v_r^{\,2}}{\epsilon_o \omega^2 U} \quad , \tag{8d}$$

with

$$\omega_p^{\,2} = \frac{q^2 N_o}{\epsilon_o m} \quad ,$$

$$\omega_h = \frac{q B_o}{m} \quad ,$$

$$N^2 = \omega_p^{\,2} / \omega^2 \quad ,$$

$$H = \omega_h / \omega \quad .$$

Upon taking the curl of (5) and the curl and divergence of (6) we may obtain the coupled wave equations

$$\nabla_\rho^2 h_z + (K_{Eo}^2 \epsilon_3 - \beta^2) h_z + i\beta \epsilon_o \frac{N^2 H\omega}{U^2} e_z + \frac{q\omega H}{U}\left(1 - \frac{\beta^2 v_r^2}{\omega^2 U}\right) n = 0 , \qquad (9)$$

$$\nabla_\rho^2 e_z + (K_{Eo}^2 \epsilon_3 - \beta^2) e_z + \frac{i\beta q}{\epsilon_o}\left(1 - \frac{K_{Eo}^2 v_r^2}{\omega^2 U}\right) n = 0 , \qquad (10)$$

$$\nabla_\rho^2 n + \frac{q}{\epsilon_o k_1}\left(\epsilon_1 - \frac{\beta^2 v_r^2}{\omega^2 U}\right) n - \frac{i\beta \epsilon_o \omega N^2 H^2}{q v_r^2 U^2} e_z + \frac{i\omega\mu_o \epsilon'}{k_1} h_z = 0 , \qquad (11)$$

where

$$\nabla_\rho^2 = \frac{1}{\rho} \frac{\partial}{\partial \rho}\left(\rho \frac{\partial}{\partial \rho}\right) ,$$

and $$K_{Eo}^2 = \omega^2 \mu_o \epsilon_o .$$

It should be mentioned that Chen and Cheng (1966) were apparently the first to derive the wave equations (7) through (9), and a similar development has been given by Mayhan and Schultz (1967). The equations are included here for the sake of completeness.

The z-components of electric and magnetic fields, e_z and h_z, and the time-varying electron number density n, are seen to satisfy coupled wave equations for the compressible magnetoplasma, given by (9) - (11). These quantities at the same time serve as potentials from which the remaining field components may be found through (1) - (4). It may be seen that (9) - (11) decouple when the static magnetic field is zero, i.e. H = 0, while for zero electron temperature, the incompressible, magnetoplasma equations are obtained.

The solution of the coupled wave equations is obtained in the standard way, by finding the eigen vectors of the coupling coefficient matrix, and obtaining then three eigen value wave equations. When the plasma is incompressible so that only two rather than three, coupled equations must be solved, the problem is considerably simplified from a numerical computation viewpoint, while for the isotropic case, only the uncoupled equations need be

treated. If a sheath is involved, then in addition to solving the wave equations for the uniform plasma medium, the sheath fields must be found. The vacuum sheath fields are obtained analytically from the free-space wave equation, where for the anisotropic plasma there are two EM modes, one the transverse electric (TE) mode with zero z-directed electric field, and the other the transverse magnetic (TM) mode with zero z-directed magnetic field. When the plasma is isotropic, only the TM mode need be considered. The inhomogeneous sheath is however considerably more difficult to treat, and the differential equations for the sheath fields must be solved by a numerical approach.

The resulting field solutions for the sheath and the uniform plasma involve constants of integration, or spectral wave amplitude coefficients in β, which are evaluated from the boundary conditions. These boundary conditions are that the tangential electric and magnetic fields be continuous across the sheath-uniform plasma interface, and that the circumferential and axial electric fields vanish everywhere on the surface of the perfectly conducting antenna except at the circumferential exciting gap, where the axial electric field is assumed equal to $-e^{i\omega t}/\delta$ with δ the gap thickness. In addition, unless otherwise indicated the radial electron velocity is assumed to vanish at the vacuum sheath-uniform plasma interface, which becomes, for zero sheath thickness, the antenna surface. This is the so-called rigid or hard boundary condition. When the inhomogeneous sheath is considered, the time-varying electron number density and radial velocity are taken to be continuous at the sheath-plasma interface, and the radial electron velocity vanishes then at the antenna surface.

The antenna admittance is obtained finally from the axial component of antenna current evaluated at the edge of the exciting gap, where the axial current is given by $2\pi c$ times the circumferential magnetic field at the antenna

surface. The admittance thus requires the inversion of a Fourier integral, the evaluation of which must be carried out numerically. Because the integrand of this integral is so complex, and due to the fact that it may be sharply peaked at a value of β corresponding to the characteristic or free waves which are excited on a source-free infinite cylinder, the success of the numerical approach is largely dependent upon the technique used for the numerical integration.

A variable-interval-width, self-convergence-checking integration technique based on the Romberg method of integration was developed for this purpose. This integration technique was found to work very well in this application, resulting in typically 100 to 150 integrand evaluations, or abscissa, points in β being required to evaluate the admittance integral with a resulting maximum-to-minimum abscissa spacing of 10^6 to 10^7. The computational accuracy of the infinite antenna admittance values to be presented should generally be better than 0.1%. Since the real part of the admittance integral, which yields the conductance, does not change sign as β increases, as may the imaginary component which gives the susceptance, the conductance values will on the whole, be more accurate. In some of the results to be presented, a small susceptance value comes from the subtraction of two nearly equal numbers, and consequently the numerical accuracy may be no better than 10 percent. Superimposed crosses will be used to denote such portions of the susceptance curves. A more complete discussion of the theoretical development and numerical computational approach is given elsewhere by one of the authors (Miller, 1967a, b, c, d). We thus prefer to omit these details here, in favor of giving the numerical and experimental results in greater detail. The calculated infinite antenna admittances are presented in Section IIb while the experiment and the results are discussed in Section III.

IIb Numerical Results for the Infinite Antenna Admittance.

The calculated infinite antenna admittance results to follow will be given first for the case of the free-space medium followed by results for the isotropic and anisotropic plasma media respectively. The free-space case is of interest to illustrate the perturbation of the infinite antenna admittance brought about by the plasma medium.

1. Infinite Antenna in Free Space.

The infinite antenna free-space admittance is shown in Fig. 1 as a function of the exciting frequency f, varying from 250 KHz to 10 MHz for an antenna of radius c equal to 1 cm and with the exciting gap thickness δ a parameter varying from 10^{-1} to 10^{-3} cm. The conductance is denoted by G and the susceptance by B, with the subscript o indicating the free-space values.

It may be seen that the conductance exceeds the capacitive susceptance over the frequency range shown, and that of the two, only the susceptance is dependent upon the exciting gap thickness. The susceptance increases with decreasing gap thickness, an effect which is more pronounced the higher the frequency. This result is not surprising since it is well-known that the susceptance of a delta-function gap is infinite, the imaginary part of the admittance integral in this case being non-convergent.

The results of Fig. 1 will be useful in showing the influence of the plasma medium on the infinite antenna admittance. The admittance results below are for an antenna of 1 cm radius and for δ = 0.1 cm. Positive susceptance values are shown as long-dashed lines and negative susceptance as short-dashed lines, with solid lines denoting the conductance.

2. Infinite Antenna in an Isotropic Plasma.

We present in Figs. 2 and 3 the infinite antenna admittance for the isotropic plasma as a function of frequency for an electron plasma frequency f_p = 1.5 MHz and an electron collision frequency $\nu = 10^4 \text{sec}^{-1}$. The results of Fig. 2 are for the sheathless case (X = 0) and those of Fig. 3 are for the vacuum sheath (X = 5), where the sheath thickness X is given in units of the electron Debye length (D_ℓ), with

$$D_\ell = \sqrt{kT_o/m} \Big/ \omega_p \ .$$

The electron temperature used to calculate the sheath thickness is $T_o = 1500^\circ K$, which results in a physical sheath thickness in this case of 0.079 m. The $T = 0^\circ K$ and $T = 1500^\circ K$ curves are for the incompressible (no EK wave is excited) and compressible plasma respectively, where we regard the electron temperature associated with the plasma compressibility and that connected with the sheath thickness as independent quantities so that the compressibility and sheath effects may be examined separately.

We observe in Fig. 2 that above f_p, the compressible and incompressible admittances differ by no more than a few percent, with the conductance and susceptance being in approximately their free-space ratio and approaching their free-space values with increasing frequency. Below f_p however, where the susceptance changes sign and the conductance is sharply decreased, the incompressible admittance is found to be monotonically increasing with decreasing frequency, while the compressible results exhibit maxima in the conductance and susceptance at roughly half the plasma frequency.

The admittance curves of Fig. 3 for the vacuum sheath are similar to those for the sheathless case of Fig. 2 when $f > f_p$, and we find that neither

the plasma compressibility nor the vacuum sheath significantly affect the infinite antenna admittance when the exciting frequency exceeds the plasma frequency. The admittance values below f_p for the vacuum sheath case of Fig. 3 are very similar for the incompressible and compressible plasmas, and resemble as well the sheathless, compressible plasma admittance curves of Fig. 2.

It appears that only for the case of the sheathless, incompressible plasma does the infinite antenna admittance lack a maximum below f_p. In addition, the effects of the plasma compressibility and vacuum sheaths, when taken separately, (Fig. 2, the T = 1,500°K curve and Fig. 3, the T = 0°K curve respectively), are found to be very similar. Finally, when both factors are simultaneously present, the admittance is little different from that obtained when each is considered alone.

In order to further see the effect the sheath has on the infinite antenna admittance, we present in Fig. 4 the admittance as a function of frequency for an inhomogeneous sheath 5–Dℓ thick in which the potential variation with ρ is taken to be parabolic with a negative maximum of -0.61V at the antenna surface. The antenna potential is calculated from a formula due to Self (1963) for an electron temperature of 1500°K and ions of atomic mass 16. The other plasma parameter values are the same as used for Fig. 2.

A comparison of Fig. 4 with Figs. 2 and 3 shows that above the plasma frequency of 1.5 MHz, and below 1.25 MHz, the inhomogeneous sheath admittance is very close in value to the corresponding results for the previous plasma models considered (except of course, the sheathless, incompressible case). In the region just below the plasma frequency however, a rather sharp conductance maximum is obtained for the inhomogeneous sheath, with a peak at about 1.35 MHz, while

the susceptance has a smaller maximum at about 1.42 MHz. This admittance resonance is a feature not exhibited by the vacuum sheath or sheathless results of Figs. 2 and 3, and would appear to indicate that a cavity-type resonance occurs in the interaction of the acoustical fields with the inhomogeneous sheath. It should be noted that wave propagation is not cutoff in the inhomogeneous sheath because of the decreasing electron density as the antenna is approached, even though $f < f_p$ in the external uniform plasma. The vacuum sheath then appears to be a rather inadequate approximation to the actual sheath inhomogeneity in the region just below the plasma frequency, for the isotropic, compressible, plasma. When the plasma is incompressible, it would seem that the vacuum sheath would not suffer this limitation, since the EM wavelength is much larger than a realistic sheath thickness, thus eliminating the possibility for an admittance resonance such as seen in Fig. 4.

3. Infinite Antenna in an Anisotropic Plasma.

The results presented in the previous section for the infinite antenna immersed in an isotropic plasma are interesting in showing the effects of the plasma compressibility and sheath, but do not realistically represent the anisotropic, ionospheric plasma. In this section admittance results are shown for the anisotropic plasma for both the compressible and incompressible cases.

Figs. 5 and 6 present the infinite antenna admittance for the anisotropic, incompressible plasma for the sheathless case, where in Fig. 5 $f_h = 1.0$MHz and $f_p = 1.5$MHz, while the values of these parameters are interchanged in Fig. 6, thus obtaining the same value for the upper hybrid frequency $f_t = \sqrt{f_h^2 + f_p^2}$ in both situations. The other parameter values are the same as used for the previous figures.

The admittance curves shown on Figs. 5 and 6 are seen to be similar in their frequency variation about f_p, f_h and f_t. When the frequency exceeds f_t, the conductance and susceptance are in approximately their free-space ratios, and approach their free-space values with increasing frequency. A conductance minimum and susceptance zero are seen at f_t, and in both cases a rather pronounced admittance maximum is found at f_h. In addition, the admittance in each case is observed to possess a minimum at f_p, that for $f_p > f_h$ occurring principally due to the susceptance and that for $f_h > f_p$ due to the conductance.

The infinite antenna admittance for the case of a vacuum sheath $5\text{-}D\ell$ thick (again calculated for an electron temperature of 1, 500°K) and the anisotropic, incompressible plasma, is presented in Figs. 7 and 8, for the same plasma parameter values as used for Figs. 5 and 6 respectively. A comparison of the admittance curves for the vacuum sheath with the corresponding sheathless results shows that the principal effect of the vacuum sheath has been to reduce in amplitude, and shift upward in frequency, the admittance maximum occurring at f_h for the sheathless case. This is a rather significant effect, and one that has been experimentally observed. The upward shift of the cyclotron admittance maximum (or impedance minimum) due to the sheath results from a series resonance between the inductive plasma and the capacitive sheath. It appears that this shift in the admittance maximum may have some potential for determining the electron temperature, since the amount of shift is evidently dependent on the sheath thickness, which is in turn a function of the electron temperature.

We turn now to the anisotropic, compressible plasma, the results of which for the sheathless case are given in Figs. 9 and 10, again for the same order of parameter values used for Figs. 5 and 6. A comparison of the admittance curves in Figs. 9 and 10 with the corresponding results of Figs. 7 and 8, shows that for the anisotropic plasma the plasma compressibility and vacuum sheath influence the antenna admittance, especially in their influence on the admittance maximum associated with f_h, in very much the same way. The isotropic and anisotropic plasmas are thus found to be alike in that the vacuum sheath and plasma compressibility influence the antenna admittance in a similar fashion.

The results just presented for the compressible anisotropic plasma are obtained for the hard boundary condition, i.e., the electrons are elastically reflected at the antenna surface, so that coupling of EM to acoustical wave energy takes place due to both the boundary condition on the electron velocity, as well as the plasma anisotropy. A pertinent question to raise at this point is, what is the relative importance of these two coupling mechanisms? Since the boundary coupling can be eliminated by considering the antenna surface to be perfectly absorbing, a surface which we refer to as a soft boundary, the use of the soft boundary condition enables us to see the effect of the magnetic field coupling alone on the antenna admittance.

Some admittance calculations were performed for this boundary condition and the sheathless, anisotropic, compressible plasma, the results obtained using the soft boundary being found to differ from the incompressible admittances by no more than a few percent. Thus the use of soft boundary in place of the hard boundary effectively eliminates the plasma compressibility from influencing the antenna admittance, even for the anisotropic plasma where magnetic field coupling is a factor.

Only the sheathless case has been thus far examined for the compressible, anisotropic plasma, because of the considerably increased computer time required for the vacuum sheath calculations for this plasma model. There is a special case of some interest which may be quite easily handled however, that of the uniaxial, compressible plasma. For this particular limit, the antenna radiates only a single EM mode, whose propagation constant contains the electron thermal velocity. The infinite antenna admittance for both the sheathless and 5-D$_\ell$ vacuum sheath cases, and both the compressible (T=1, 500^{o}K) and incompressible (T=0^{o}K) uniaxial plasmas, is shown in Fig. 11.

We observe first of all that the conductance is the same for all four cases shown, and exhibits a minimum at f_p very similar to that found in Figs. 8 and 10 respectively for the incompressible and compressible anisotropic plasmas, with $f_p < f_h$. The susceptance is seen to be positive (capacitive) above f_p and very little different for all four cases also. Below f_p however, the effect of the vacuum sheath is seen to be rather pronounced, the sheathless susceptance becoming inductive then, while the vacuum sheath susceptance becomes abruptly smaller at f_p but still remains capacitive with decreasing frequency. It is significant to see that only the susceptance is sensitive to the electron temperature, and even that only slightly, so that because the conductance is considerably larger, the admittance magnitude is not influenced by the plasma conpressibility.

It is now pertinent to ask what are the implications of the infinite antenna admittance results in connection with the operation of a finite antenna in the ionosphere. Because the ionosphere is an anisotropic plasma, our answer to this question must be based principally on the admittance curves presented in

section 3. Upon reviewing the effects of the plasma compressibility, the sheath and the plasma anisotropy on the infinite antenna admittance, we find that when the frequency is larger than approximately 1.5 f_h (for the f_p values used here), the admittance in all cases considered is well represented by that obtained for the incompressible, sheathless plasma. It thus appears that for the frequency range $f > 1.5\ f_h$, a finite antenna theory for a "cold" or incompressible plasma which disregards the sheath, such as that due to Balmain (1964), may be adequate for predicting the impedance characteristics of a finite antenna in the ionosphere.

If we consider the frequency range near f_h, it is apparent however, that some account must be taken of the plasma compressibility and sheath. It may be remarked in this regard that while the plasma compressibility and vacuum sheath, when considered separately, affect the infinite antenna admittance in a similar fashion for both the isotropic and anisotropic plasmas, the influence of the compressibility is quite likely over-emphasized by the hard boundary condition. This fact, as well as the results presented above which show that when there is a sheath present, the compressible admittance variation with frequency is not significantly different from that for the incompressible case, indicate that the sheath is more important than the plasma compressibility. An interesting experiment suggests itself here, of biasing the plasma-immersed antenna to the point of sheath collapse, so that any shift of the admittance maximum away from f_h may provide evidence of plasma compressibility.

For purposes of comparison, we now present in Figs. 12 and 13, the admittance of a finite cylindrical dipole antenna of half-length $h = 3.048$m (10ft) and radius $c = 0.01$ m, calculated from Balmain's (1964) quasistatic formula for the antenna parallel to the static magnetic field. The plasma parameter values used in obtaining the results on Figs. 12 and 13 are the same as used for Figs. 5 and 6 respectively.

It may be observed that the finite antenna admittance shown in Figs. 12 and 13 are qualitatively very much like the corresponding infinite antenna results of Figs. 5 and 6. The basic features of the two sets of admittance curves are especially alike in the region of cutoff wave propagation in the axial or z-direction, defined by $f_h < f < f_t$. This is not surprising since the antenna end-effects become less important then. It is rather interesting to see that the quasistatic formulation for the finite antenna and the rigorous boundary value approach for the infinite antenna are substantially in agreement. The experimental results to be given in the next section will provide further evidence for the validity of Balmains quasistatic impedance formula, as well as the qualitative correctness of the infinite antenna analysis.

III. Ionospheric Measurements

IIIa. The Experiment.

The theoretical analysis described above was prompted by the requirement for a simple and reliable method to obtain electron density altitude profiles. Historically, many methods both simple and complex have been used with varying degrees of success. When an ionosonde cannot be used because of ionospheric disturbances or F2 peak height limitations, the investigator generally must resort to direct probing with rocket vehicles. In this case, techniques which are sensitive to vehicle plasma sheath or wake effects should be avoided if possible. This leads naturally to RF probe techniques, which can detect the local electron plasma frequency in a region not just bounded by the sheath, and from which electron density can easily be calculated. Heikkila, et al. (1967) describe several RF probe techniques and discuss their advantages and limitations. By a fortunate coincidence, we elected to study and develop further, three of the techniques discussed in the reference. The experiments were successfully flown to 292 kilometers aboard an Aerobee rocket (NASA 4.207) on 8 August 1968 at White Sands, New Mexico.

Figure 14 depicts the rocket payload after nose cone ejection and antenna deployment. Beginning at the rocket tail is a fin-mounted notch antenna for a standard IRIG FM/PM 2 watt telemetry data transmission. Near the base of the experiment payload section is the 4.58 meter half length balanced electric dipole. The antenna elements are thin beryllium-copper tubes approximately 2.0 cm in diameter. After the rocket is despun to 1/3 RPM, at 120 kilometers, antenna element deployment begins and is completed 25 seconds later at 165 kilometers. Proceeding noseward, the next item shown is a solar sensor for determination of vehicle - sun aspect. Above the solar sensor is an open

ion source quadrupole mass spectrometer for measurement of atmospheric composition. The instrument is a dual mode device, capable of sequentially measuring neutral and ionic species from mass 1 to mass 44. The two short probes above the mass spectrometer are mounted 180^{o} in azimuth from each other and are in the plane defined by the rocket longitudinal axis and the extendable dipole antenna. One probe is a guarded cylindrical Langmuir probe for measurement of electron temperature, density and vehicle potential. The other probe is used as a very short whip antenna to monitor the RF field induced by the dipole antenna. Above the probes, the nose-cone ogive is truncated and fitted with a cylindrical section which contains a completely self-contained mass spectrometer and telemetry system. This experiment package and its covering nose-cone is ejected before antenna extension commences and is many vehicle lengths away when extension is complete. The object of the ejectable spectrometer is to compare its results with the non-ejected instrument and search for local vehicle outgassing and contamination effects, if any. Also mounted in the forward cylindrical section are two mutually perpendicular magnetometers to measure the vehicle orientation with respect to the local earth's magnetic field.

Accurate determination of ambient of electron density profiles, in addition to being useful in its own right, is also necessary when reducing ion spectrometer data to useful atmospheric ion number densities. The RF probes were included to obtain electron density profiles, compare data obtained from each, and also to compare their results with those from the Langmuir probe and a ground-based ionosonde. The technique judged most successful in producing reliable results without excessive experiment complexity will be selected for further refinement and routine use. The other instruments shown in Fig. 14 do not pertain to this topic and thus will not be discussed further here.

The balanced dipole antenna is itself the sensor for two of the probe experiments. In both cases, the dipole is excited with a carefully balanced with-respect-to-ground swept-frequency voltage of approximately 4 volts RMS. Both phase and amplitude balance are carefully controlled, and the frequency is continuously varied from 0.8 to 10 MHz. This range enables us to measure from well below the cyclotron frequency to well above the plasma frequency over the complete altitude range of the rocket trajectory. For convenience, the frequency range is divided into two over-lapping bands, from 0.8 to 3.5 MHz and from 2.6 to 10 MHz. The two ranges are repeated in sequence and each sweep requires approximately 2 seconds. Forty two complete sweeps were obtained after antenna deployment on the upleg and fifty two sweeps were obtained on the downleg until antenna breakup occurred during payload reentry.

The first RF probe technique we describe is an attempt to detect the slowly decaying plasma oscillations of the type observed by the Alouette and Explorer XX satellites. These resonances occur at the plasma frequency f_p, at the electron cyclotron frequency f_h and at the upper hybrid frequency f_t. An experiment of this type has been called a "resonance relaxation probe" by Heikkila. Although there is general agreement that local plasma frequencies determined in this manner lead to accurate values of ambient electron density, a disadvantage of the technique is its complexity. A complete, miniaturized ionosonde must be flown. Since this is often impractical, a major simplification of the technique was attempted with the relaxation resonance probe. This was accomplished by connecting a simple, untuned difference frequency detector to the antenna terminals. As the antenna excitation frequency sweeps through its range the plasma is excited into resonance when the sweep reaches f_p. As the excitation frequency continues to increase, two frequencies are

present at the antenna terminals, the higher excitation frequency and a low-level signal coupled into the antenna from the decaying plasma response. The difference detector has high sensitivity, wide dynamic range and is designed to respond only to the difference between the two frequencies. In principle, this detector should produce a rapidly rising audio output signal, starting from 0 Hz. In practice, responses below about 100 Hz are attenuated and the high frequency limit is adjusted to be less than 10 KHz because of the expectation that the plasma will decay to an undetectable level before that point is reached. Typical ionospheric responses produced by the probe are shown in the following section. Because they are more complex than were expected, they have not yet been fully analyzed.

The second RF probe involves both the main balanced dipole and the short probe located above the non-ejected mass spectrometer. A high input impedance untuned video amplifier-detector connected to the probe monitors the signal level induced by the main antenna. It is thus a type of transmission experiment although it should be recognized that over much of the sweep frequency range, the probe is well within the near field region of exciting dipole. Signal level variations at f_h, f_p, and f_t have been observed in experiments of this type. Heikkila has called this a mutual admittance measurement, although in his case, the detector was tuned to respond only to signals at the exciting frequency only. As in the first experiment, typical responses are shown in the next section; analysis of the data is continuing and will be reported on elsewhere when this work is completed.

The third experiment also involves the use of the antenna itself as a sensor. In this case the absolute magnitude of the antenna impedance is continuously measured over the complete sweep range by measuring the voltage

applied, and the current flowing to the antenna terminals. For convenience, and because of the balanced dipole symmetry, only the current and voltage to one half of the antenna is measured. This causes the effects of the vehicle wake and sheath variations with stream angle of attack to be more evident, but these perturbations are not serious. The phase angle between voltage and current is not measured. The experimental and numerical impedance results presented below thus pertain to a half-dipole or the equivalent monopole antenna. This technique can also be characterized as a type of admittance probe.

Fig. 15 is a schematic of the three probes described above. The current transformer shown in series with one antenna terminal is a low impedance device that introduces negligible impedance in series with the antenna and less than 1 $\mu\mu$f of capacitance in shunt to ground. Great care is exercised in maintaining balanced excitation and stray capacitance on each side of the antenna to ground. It is also necessary to carefully measure the stray capacitance to ground during preflight calibration of this experiment. More will be said about this later. The resistors in series with the sweep generator output leads are necessary to prevent the relaxation resonance signals from being shunted to ground by the low impedance of the output amplifiers of the generator. As the antenna impedance varies over the excitation frequency range, the resistors cause a voltage divider action to occur and thus the antenna terminal voltage as well as current varies with antenna impedance changes. This is not a problem however because again, preflight calibration provides adequate information to correct for the effect.

IIIb. Impedance Results.

In Figure 16a, a section of the original flight telemetering record from these experiments is shown. There are two records, since as discussed above, the overall 0.8 to 10 MHz frequency range was covered in two overlapping

sweeps. In each record, the two outer traces on top and botton are timing and trace deflection reference lines. The top data channel, labelled No. 1 is the output from the resonance relaxation detector which operated simultaneously during the impedance measurement. Channel No. 2 below it is the output from the small probe near the tip of the rocket. An upward deflection indicates an increase in the detected signal level. Abrupt responses are apparent on both upper traces as well as on all other frequency sweeps throughout the flight. Some are particularly remarkable, but since they have not yet been fully analyzed the remaining discussion is confined to the antenna impedance results.

Channels 3 and 4 are antenna current and voltage respectively with upward deflections indicating an increase in magnitude of the parameter. Channel No. 5 is a ramp function whose deflection is related to the excitation sweep frequency. It is important to note here that the records in Figure 16 are plotted with a uniform time base as the abscissa. Some deviation from linearity of sweep frequency with respect to time exists in both sweeps on these records. Channel 5 was intended to provide the time-to-frequency conversion function but the residual telemetering noise on this channel generated prohibitivity large conversion errors during some portions of the sweep. Crystal controlled marker frequencies which were inserted periodically throughout the flight on Channel 1 were used instead to provide the final time to frequency conversion.

Shown near the right hand side of the high frequency sweep is the typical artifact which occurs when the telemetering signal is lost due to rocket telemetering antenna pattern nulls. These events were very rare during this flight. Although not shown on this record, periodic in-flight calibration of the

telemetering system also occurred every 60 seconds. The small random fluctuations on all five channels are due to the overall system signal-to-noise ratio, but the fine detail which has a more coherent pattern is believed to be real. Comparison of many successive sweeps and the amount of scatter in the final results form the basis for this interpretation.

During flight the received data are recorded in real time both in the form shown in Fig. 16a and on magnetic tape. Later the taped data were played back into a high speed analog to digital converter which sampled each channel 833 times each second. Computer reduction of the data then followed, with all calibration and timing being included as required. Antenna impedance was calculated and the data were then plotted by machine.

Figure 16b shows an 833 sample per second antenna impedance plot calculated from the data in Figure 16a. A uniform time abscissa is used for convenience and again the data are unsmoothed and no points have been deleted. It may be seen that there are almost 1800 data points per sweep and although it is not readily apparent because of the narrow spacing between each sample, straight lines have been drawn by the plotter between adjacent data points.

With the use of the frequency marker generated calibration curves, it is an easy matter to identify the various frequencies of interest on the computer plotted curve, while at the same time the generation of an impedance vs. frequency curve is straightforward, the result of which for Fig. 16b is shown in Fig. 16c. It should be noted that the curve in Fig. 16c is a smoothed version of 16b in that the oscillations in the impedance magnitude due to telemetry noise have been averaged out, but an attempt has been made to preserve the essential features of the impedance results. Because the experiment was carried out by sweeping the frequency rather than making the measurement at a fixed number of frequencies, we present the experimental impedance as a continuous curve.

On this one plot also are shown the separate curves obtained from the low and high frequency sweeps in the region where they overlap. Quite good agreement was obtained between the overlapping low and high frequency sweeps, and on subsequent graphs only a single curve will be shown.

Also included on the experimental half dipole impedance plot of Fig. 16c, which was taken on the downward leg of the flight at an altitude of 260 to 256 km, is a theoretical curve calculated from Balmain's (1964) quasistatic formula for a monople antenna 4.58 m long and 0.01 m in radius, the values appropriate for the antenna used in the experiment. The parameters used to obtain the theoretical curve are f_p = 3.75 MHz, f_h = 1.25 MHz and $\nu = 10^6 \text{sec}^{-1}$ for the antenna parallel to the static magnetic field. The data points shown on the theoretical curves are the frequencies at which the impedance was calculated.

Before remarking on the way f_p and ν were chosed, it is pertinent to remark that the antenna impedance peaks considerably below the upper hybrid frequency which in this case would be f_t = 3.93 MHz. This downward shift of the upper hybrid resonance is caused by the stray shunt capacitance C_s of the antenna deployment mechanism and the small portion of antenna inside the rocket near the rocket casing. This shunt capacitance, of about 26 $\mu\mu$fd, produces a parallel resonance with the inductive antenna reactance in the frequency range $f_h < f < f_t$, so that the impedance maximum occurs below f_t. The shunt capacitance, which is included in the theoretical curve for the plasma-immersed antenna, also reduces the free-space antenna impedance, the theoretical values for which, both with and without the effect of C_s, are also shown in Fig. 16c.

The experimental data for the impedance provides two for the most part self-consistent methods for obtaining f_p. First of all, since the location in frequency of the impedance peak is a function of f_p, f_h and C_s, a knowledge of C_s, which is determined experimentally and f_h which may be measured in

flight, means that the remaining parameter, f_p, may be calculated from the frequency of the impedance peak. The method it should be remarked, does not depend on the absolute magnitude of the impedance.

A second possibility for determining f_p is comparing the measured impedance magnitude at a given frequency with a theoretical curve of impedance magnitude as a function of f_p at that frequency. The frequency chosen for this method of obtaining f_p should ideally be greater than f_t, since it appears that the quasistatic theory is most valid in this frequency range, but should on the other hand not exceed f_t by too much since the impedance sensitivity to f_p decreases as f/f_t increases. The frequency used in applying this method of finding f_p is 5.25 MHz, chosen partly because it exceeds the largest f_t value encountered in the experiment, and also because this was the value of one of the marker frequencies, so that the frequency could consequently be very accurately determined.

Fig. 17 shows the resulting theoretical curves for determining f_p by the methods mentioned above. The theoretical sets of curves are both calculated for h = 4.58 m, c = 0.01 m, $\nu = 10^4 \text{sec}^{-1}$, f_h = 1.25 MHz and θ, the angle of the antenna with respect to the static magnetic field, is zero, while C_s is a parameter with the values 20, 24 and 28 $\mu\mu$fd. The values obtained for f_p from these two methods were generally within 5 percent over most of the rocket flight with the best agreement occurring near apogee.

The theoretical curve shown on Fig. 16c was obtained by varying f_p between the two f_p values obtained from the frequency of the impedance peak and the impedance value at 5.25 MHz, while also varying ν, to get the best overall agreement between the theoretical and experimental results. It may be seen that the theoretical and experimental impedances are in quite good agreement for frequencies greater than the impedance peak at about 3.4 MHz.

The theoretical curve is considerably different from the experimental curve in the lower frequency range however, the theoretical impedance minimum being located at f_h while the experimental value is shifted upwards to about 2.35 MHz. In addition, the experimental impedance exhibits a small perturbation at a frequency of approximately 2.6 MHz which is not seen in the theoretical curve. An impedance perturbation at the same general frequency, approximately 2 f_h, was seen consistently in data obtained at altitudes above 200 km.

It thus appears that Balmain's (1964) quasistatic theory, while not predicting some of the experimental impedance features, does provide a reasonably accurate picture of the impedance of a plasma-immersed antenna at frequencies greater than approximately 2 f_h. This is roughly the frequency range where the infinite antenna admittance was found to be relatively unaffected by the plasma compressibility and sheath.

The upward shift of the impedance minimum from f_h is evidently due to a sheath and/or the plasma compressibility, as evidenced by the infinite antenna admittance results previously given. In order to further demonstrate this, Fig. 18 shows the impedance of an infinite monopole antenna of radius c = 1 cm and exciting gap thickness $\delta = 5\times10^{-2}$cm, for f_p = 4 MHz, f_h = 1.25 MHz, $\nu = 10^4 \text{sec}^{-1}$ and a vacuum sheath thickness X of 7 D_ℓ for an electron temperature of 1,500°K. This sheath thickness is equivalent to an electron temperature of 2,500°K with X = 5.42 D_ℓ. Two curves are shown on Fig. 17, one with C_s = 26 $\mu\mu$fd, the value appropriate for the actual experiment, and the other with C_s = 126 $\mu\mu$fd, increased in proportion to the amount the infinite antenna susceptance exceeds the finite antenna susceptance in the plasma medium at 3.0 MHz. This latter case is included to show the shift in the infinite antenna impedance peak due to C_s in a manner corresponding to the actual experiment.

The theoretical curves are both seen to have an impedance minimum at 2.3 MHz. As expected, the C_s = 126 $\mu\mu$fd curve peaks at a lower frequency, about 3.3 MHz, than that for the lower value of C_s which peaks at about 3.9 MHz. Also observable is a slight discontinuity in slope of the 126 $\mu\mu$fd curve at the plasma frequency of 4.0 MHz, while on the other curve, the effect is more pronounced, there being a slight impedance minimum at f_p.

It is interesting to note that an impedance discontinuity at f_p has been reported by Heikkila et. al. (1967) in some experimental impedance measurements in the ionosphere. This feature of either a discontinuity or impedance minimum has also been quite frequently observed in the impedance results of the present rocket flight, the values of f_p obtained as a result being generally within 5 to 10 percent of those obtained by the other two methods outlined above. The experimental impedance curve of Fig. 16c is seen to possess a discontinuity at a frequency of 3.4 MHz. It is apparent that the shunt capacitance, besides shifting the impedance peak downward in frequency, decreases the effectiveness of the impedance discontinuity at f_p, as shown by the two curves of Fig. 18.

In the concluding set of graphs, we present in Fig. 19a through e the experimental impedance vs. frequency curves for a number of altitudes on the downward leg of the flight. Also shown on the graphs are theoretical curves calculated from Balmain's (1964) formula, using values of f_p and ν which appear to give the best overall fit to the experimental values. The theoretical impedances are obtained for $\theta = 0^o$ except where otherwise indicated.

The experimental impedance vs. frequency curves are seen to exhibit some consistent trends as the altitude of the antenna decreases. First of all, the frequencies at which both the impedance minima and peak occur are seen to decrease with decreasing altitude. In addition, the minimum impedance

value may be seen to increase with decreasing altitude while the peak value decreases, so that the impedance variation with frequency is considerably reduced at the lower altitudes.

A consequent reduction in the plasma frequency and sheath thickness, and increase in collision frequency as the altitude decreases is thus indicated. We should mention that while the experimental curves of Fig. 19 are typical samples of the impedance results obtained, principally in possessing one well-defined impedance peak, some of the impedance curves were found to have two or three less prominent, but apparently real, peaks.

The degree of conformity between the experimental and theoretical results of Fig. 19 is on the same order as that seen in the previous curves of Fig. 16c. In particular, we see that the experimental impedance variation at the peak is fairly well represented by the theory, but in the frequency range greater that 4 to 5 MHz to about 6 MHz, the theoretical impedance is slightly less than the experimental value. Below 2.5 to 3.0 MHz, the upward shift in frequency of the experimental impedance minimum which the theory predicts at f_h results in a large discrepancy between the theoretical and experimental impedance values. The results of Fig. 19 thus further corroborate the conclusion reached from the findings of Fig. 16c that Balmain's quasistatic theory is reasonably valid for frequencies exceeding 2.5 to 3 MHz (approximately 2 f_h).

We have so far discussed the uncertainties in the experimental impedance results due to the measuring circuits, telemetry noise, etc., which must be considered in comparing the experimental and theoretical impedances. We have not however considered many of the factors involved in the actual experiment which are difficult to account for theoretically in even an approximate way, and which may therefore account for some of the discrepancy between the experiment and theory. During one complete frequency sweep for example, which takes about 4.3 seconds, the rocket rotates

about its axis more than 90^{o} and may more a vertical distance of more than 5 km. Consequently, the plasma seen by the antenna is not constant, but may change significantly in the course of even a single frequency sweep.

Among the more important effects which may arise due to the antenna motion, besides the obvious one of the changing values of f_p and f_h with altitude in the ionosphere, are the varying orientation of the antenna with respect to the static magnetic field and the rocket wake. As shown by the theoretical curves of Fig. 19, the impedance peak may be rather significantly shifted in frequency as θ varies from 0^{o} to 90^{o}, since the susceptance is quite sensitive to θ for the range $f_h < f < f_t$. A better fit to the experimental data may thus be obtained by using the actual time-varying value of θ, as well as the altitude-dependent value of f_h in the calculations. The magnetic field orientation of the antenna may also indirectly influence the impedance through the effect of the magnetic field on the sheath. Finally it should be noted that the impedance discontinuity or minimum at f_p is more pronounced as θ approaches 90^{o}.

The orientation of the half-dipole antenna with respect to the rocket motion, whether for example it faces into the direction of motion and views as a result the unperturbed ionospheric plasma, or trails the rocket and is located in its wake, may also be expected to influence the impedance. As a matter of fact, the 5.25 MHz impedance values have been found to vary with the period of the rocket retation, and to be well correlated with the velocity component of the rocket tangent to the antenna.

Besides the fact that the actual plasma differs considerably from the idealized model used in the theoretical analysis, there are the physical parameters of the antenna length and radius, and the shunt capacitance, any error in the values of which may cause the theoretical impedance to vary from the measured values. The antenna consists of a rolled up metal strip which

curls over as it deploys to form a hollow tubular cylinder. The radius and length of the antenna can be accurately measured on the ground but the total length of antenna actually deployed may differ by a few cm from the measured value, while the length and radius are also functions of the antenna temperature in the ionosphere. Since the theoretical impedance is inversely dependent on the antenna length, and because in addition the impedance is much more rapidly changing in the range of the impedance peak than in the range $f > f_t$, an error in the value of h used for the theoretical calculation will result in a larger relative error in the value of f_p obtained from the 5.25 MHz impedance than the frequency of the impedance peak and its corresponding f_p value.

In addition, C_s is an important parameter as illustrated by Fig. 17 and an error in its value would primarily affect the frequency of the impedance magnitude at 5.25 MHz. It should be mentioned also that the measured value of C_s was found to increase slightly with increasing frequency, indicating a lossy component, so that a more accurate shunt impedance would be a capacitor and resistor in series. The value of C_s used in the calculations is an average of the measurements at 5.25 MHz.

The telemetry system, laboratory calibrations, in-flight parameter drifts and data processing procedures all introduce some error into the final results. It is not a simple task to accurately assess the overall effect of even an equal magnitude error in each of the above items because of the complex magnitude versus frequency transfer function of the total system. We estimate however that the results presented here lead to plasma frequency determinations with an error of less than ± 10 percent. The largest error in impedance magnitude occurs at the impedance peak near f_t but as pointed out above, it is the frequency at which the peak occurs and not its magnitude which is the important parameter. Frequency can be determined with an accuracy of better than ± 1 percent.

Upon taking all of these factors into consideration the relative agreement obtained between the theoretical and experimental impedance results seems to provide good evidence for the basic validity of the theoretical approach incorporated in both the infinite antenna study and Balmain's quasistatic analysis. It appears that accounting for the altitude and time variation of the static magnetic field, and allowing for a complex shunt impedance may further improve the agreement of theory and experiment. It is at the same time apparent that in order to satisfactorily account for some of the features exhibited by the experimental impedance results, an extension of the theory to consider more realistically the actual experimental conditions, such as the rocket wake and plasma inhomogeneity, is required.

Conclusion

We have presented here the results of a theoretical investigation of the admittance of an infinite cylindrical antenna immersed in an ionospheric-type plasma. The infinite antenna study indicates that the ion sheath and plasma anisotropy are more important than the plasma compressibility in affecting the behavior of an antenna in the ionosphere. Based on the infinite antenna findings and a comparison with Balmain's (1964) quasistatic impedance formula, it is concluded that the impedance of a finite antenna in the ionosphere is well represented by Balmain's quasistatic formula for frequencies exceeding 1.5 to 2 f_h.

A comparison of the experimental impedance measurements of a rocket-borne antenna in the ionosphere with values calculated from Balmain's formula shows that quite good agreement is obtained for frequencies greater that 2.5 to 3 MHz (approximately 2 f_h). There is a discrepancy between the experimental and theoretical results for frequencies in the vicinity of f_h which is apparently due to the sheath, a factor which Balmain's formula does not include. The experimental impedances are found to provide two generally self-consistent methods for determining f_p, one based on the frequency at which an impedance peak occurs, and the other on the impedance magnitude at a given frequency which exceeds the upper hybrid frequency. A third method which yields f_p is the frequency at which an impedance discontinuity or minimum occurs. A disadvantage of this method is the difficulty often encountered in identifying this point on the impedance curve. The electron density profile derived from the RF probes compares very favorably with data obtained from a ground-based ionosonde taken at the time of the flight.

In conclusion, we may remark that, considering the variation of the actual plasma encountered experimentally from that treated theoretically, the relative agreement between experiment and theory indicates that the basic physics of the problem are incorporated in a fairly realistic way in the theory. A further refinement of both the theoretical approach to allow for the inhomogeneous plasma near the antenna which results from the antenna sheath and rocket wake, as well as including in the present theoretical calculation the time variation of the parameters θ, f_h and f_p resulting from the antenna motion during a frequency sweep, may be expected to further improve the agreement between theory and experiment.

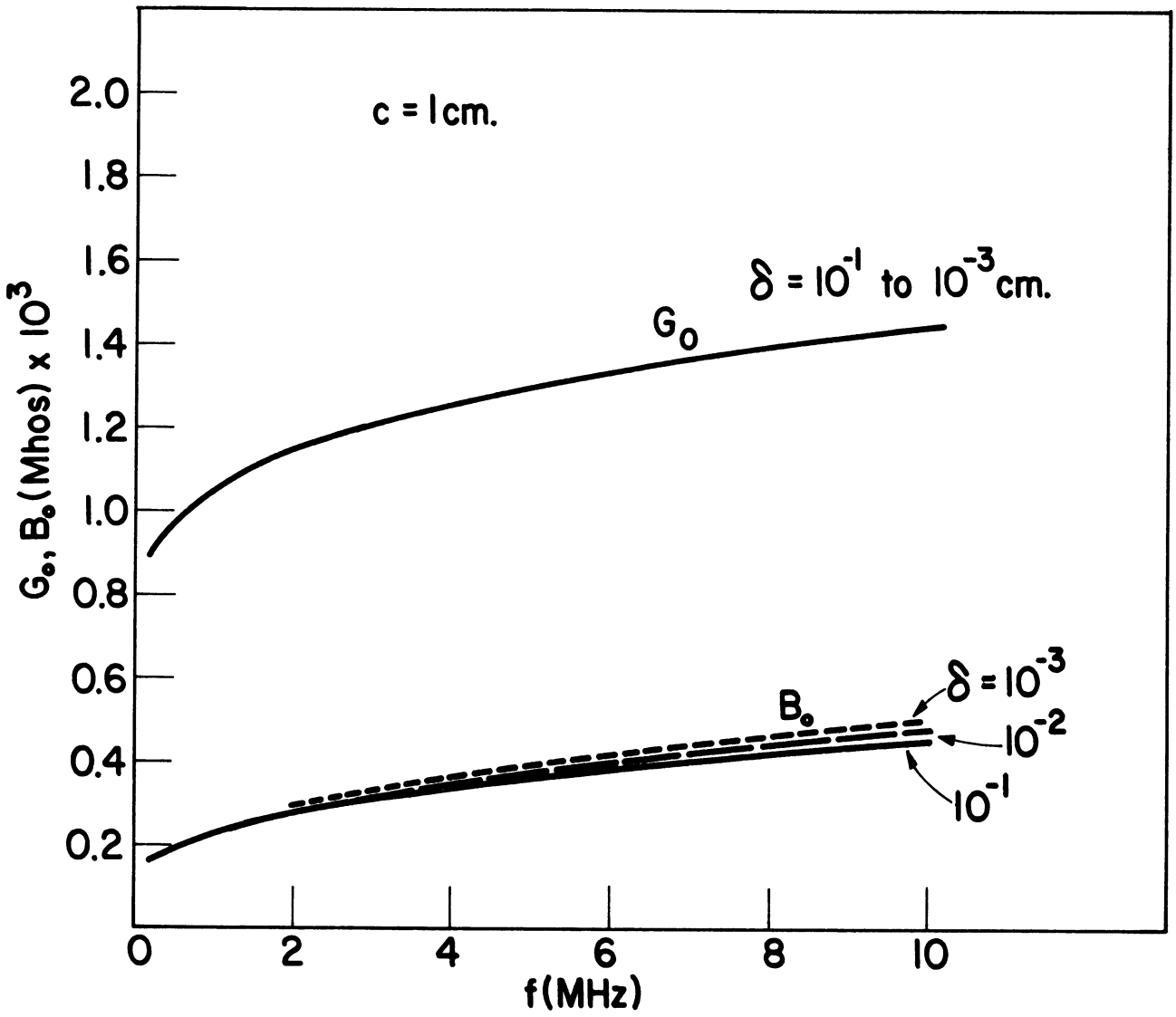

Figure 1. The free-space infinite cylindrical antenna admittance as a function of frequency with the exciting gap thickness, δ , a parameter and a radius, c, of 1 cm.

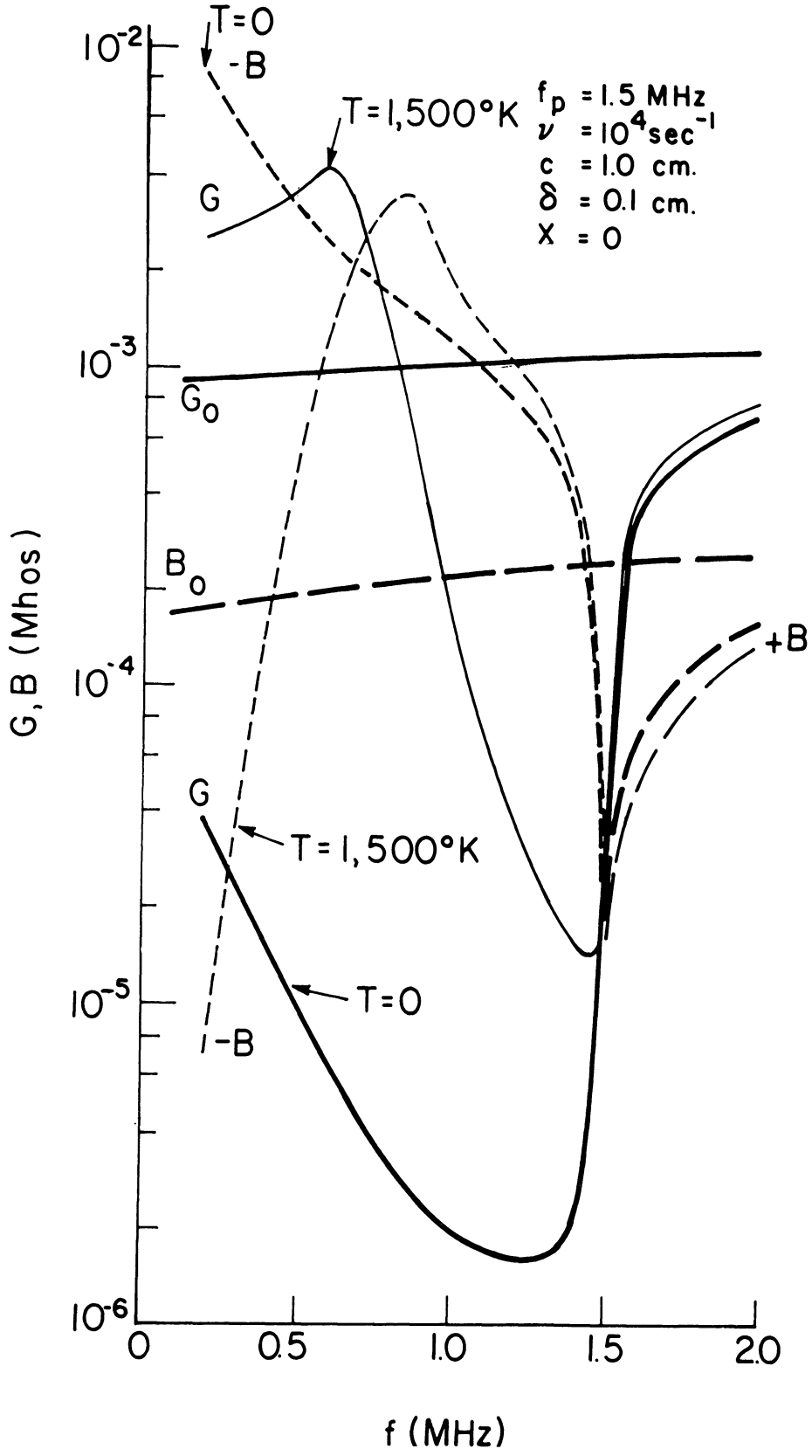

Figure 2. The infinite antenna admittance as a function of frequency in an isotropic plasma for both the compressible (T=1500°K) and incompressible (T=0°K) cases and zero sheath thickness with an electron plasma frequency of 1.5 MHz.

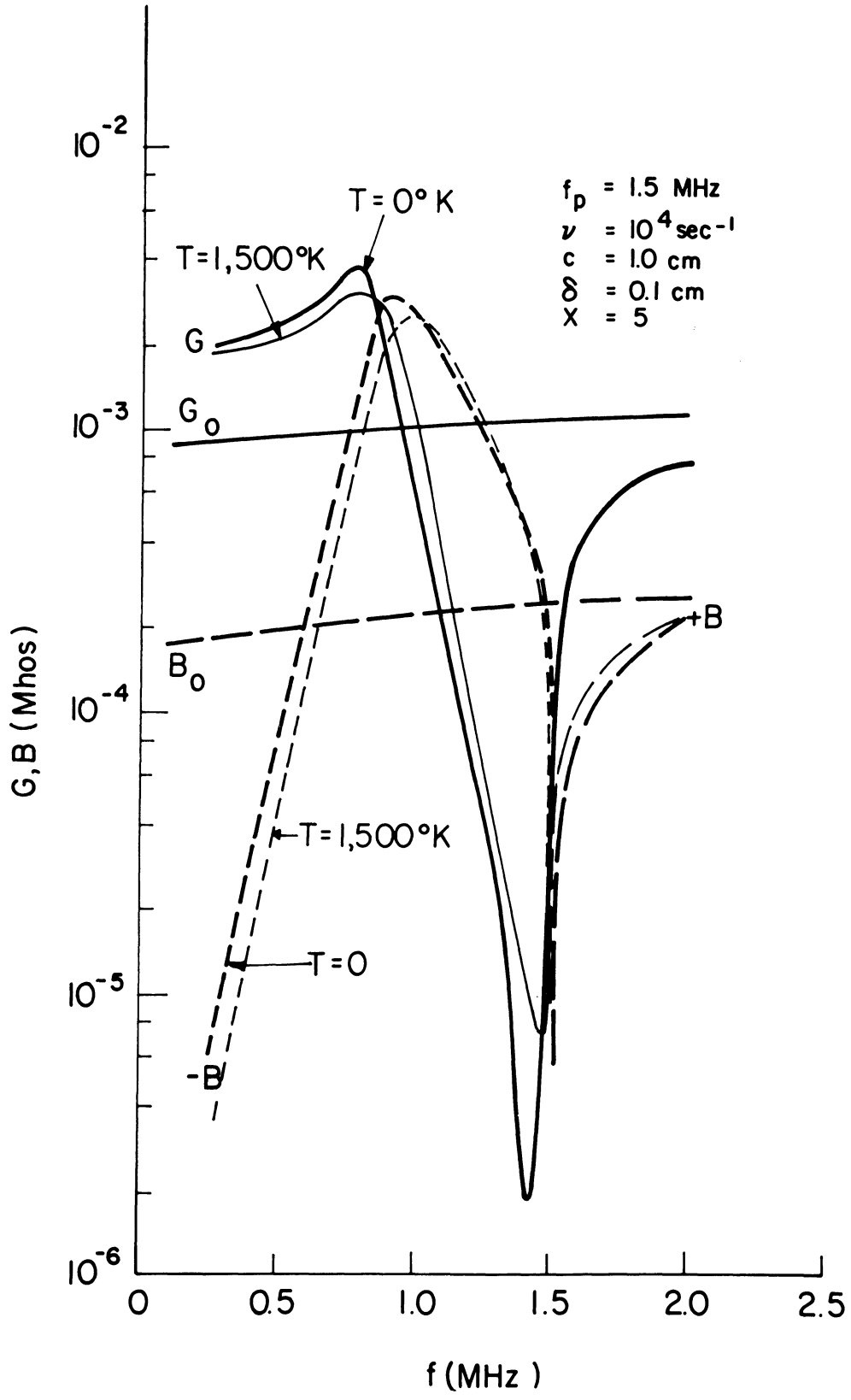

Figure 3. The infinite antenna admittance as a function of frequency in an isotropic plasma for both the compressible (T=1500°K) and incompressible (T=0°K) cases and a vacuum sheath thickness of 5 D_ℓ with an electron plasma frequency of 1.5 MHz.

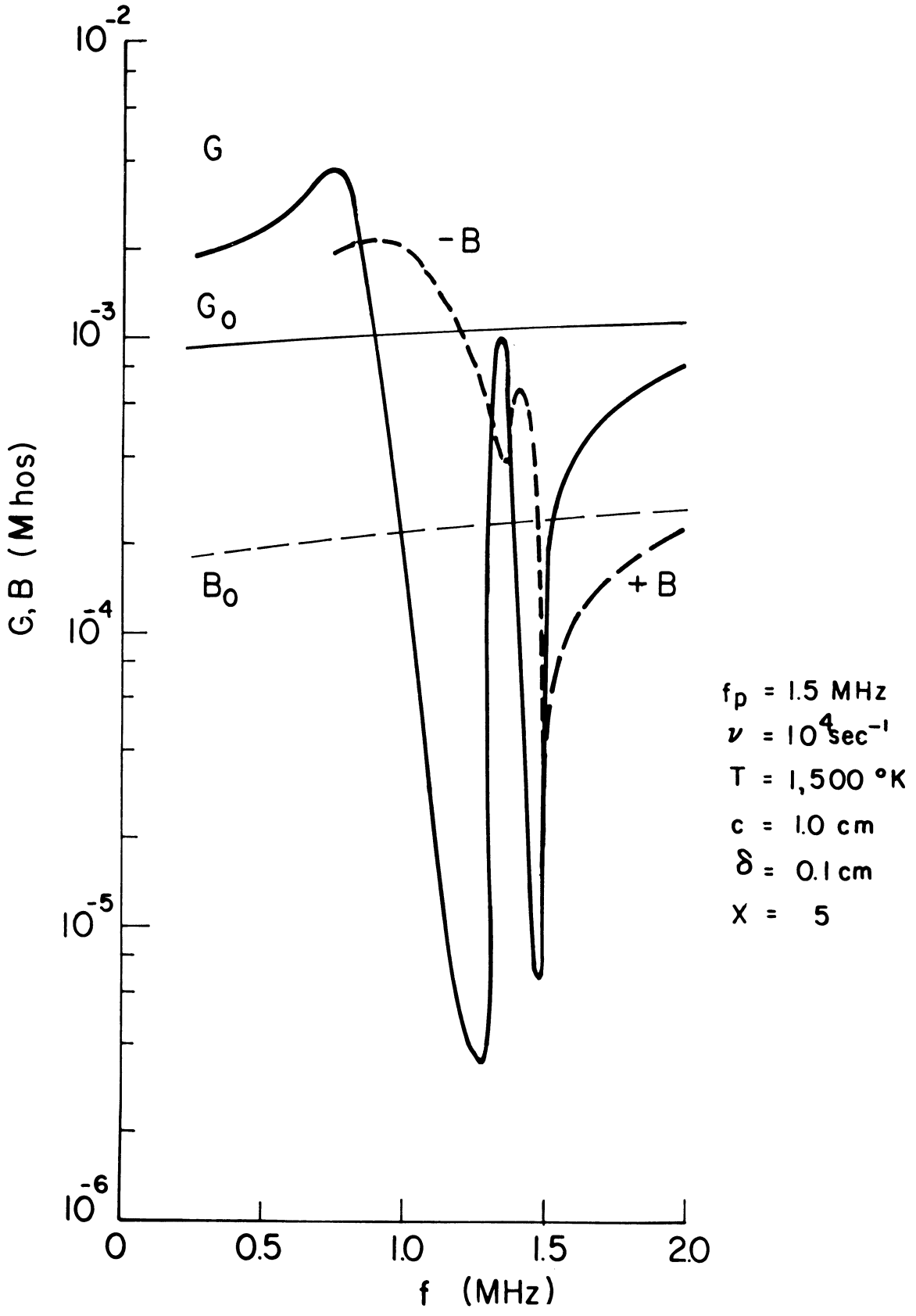

Figure 4. The infinite antenna admittance as a function of frequency for an isotropic, compressible plasma with an inhomogeneous sheath 5 $D\ell$ thick and an electron plasma frequency of 1.5 MHz.

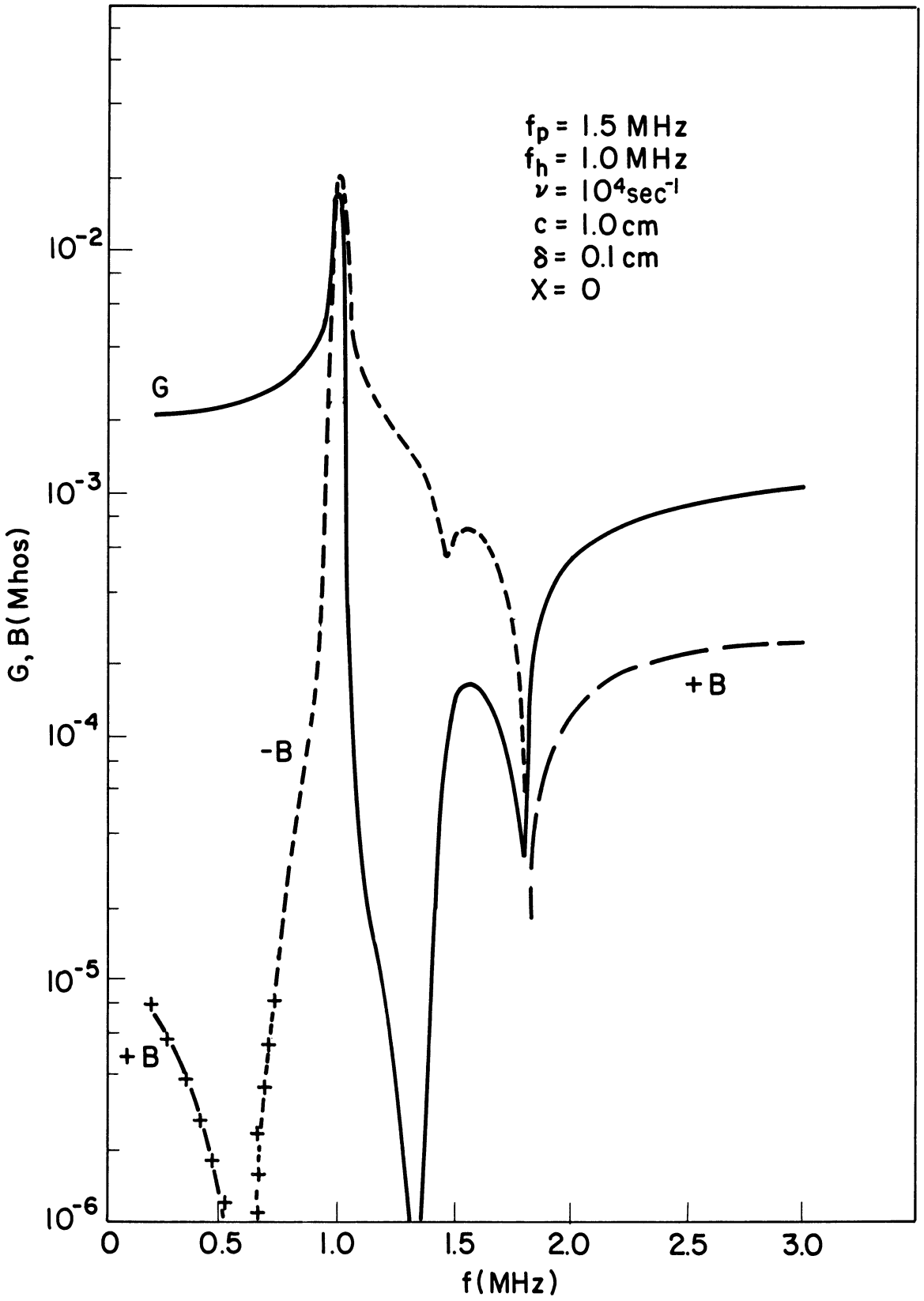

Figure 5. The infinite antenna admittance as a function of frequency for the incompressible magnetoplasma and the sheathless case, with an electron plasma frequency of 1.5 MHz and electron cyclotron frequency of 1.0 MHz.

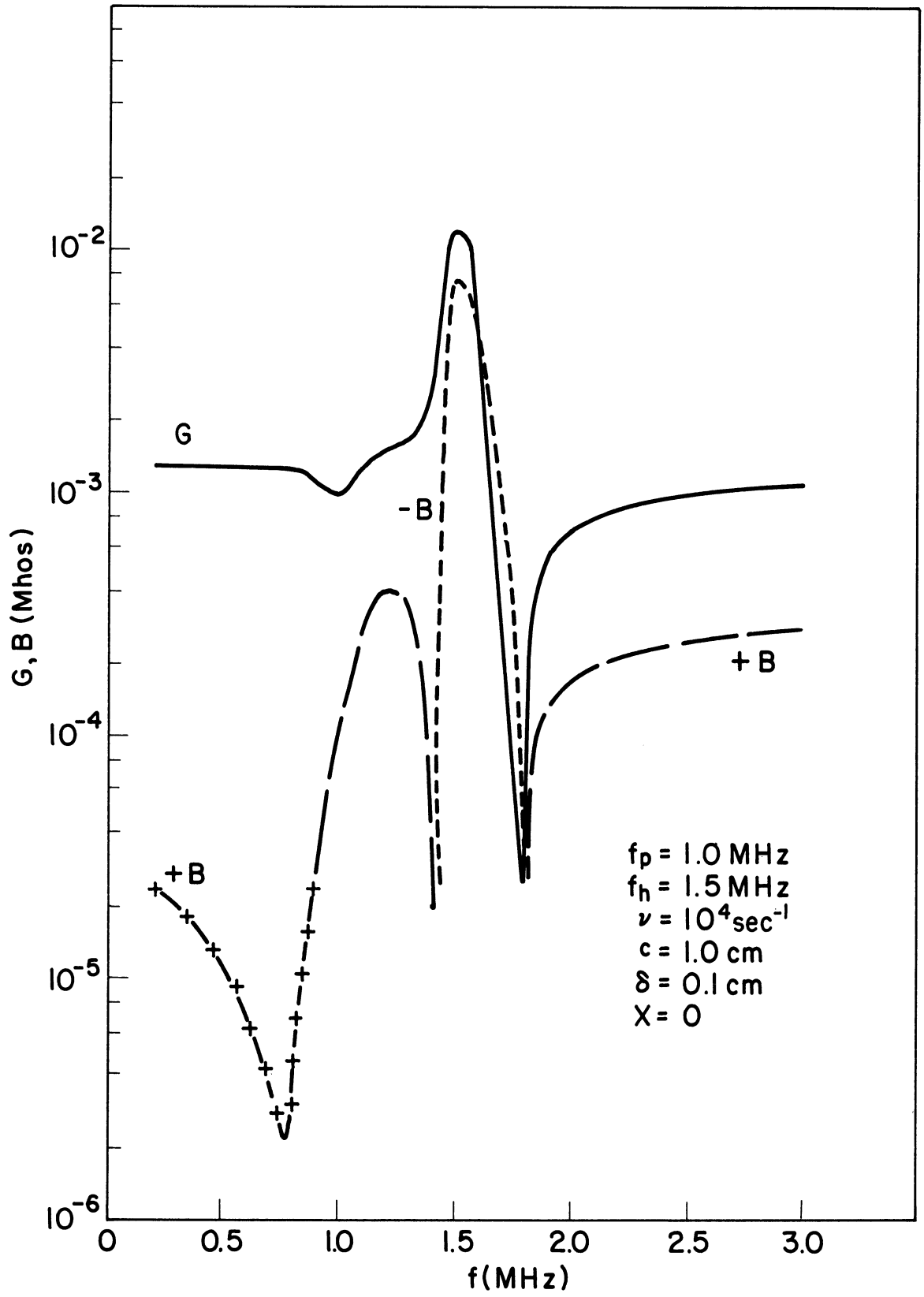

Figure 6. The infinite antenna admittance as a function of frequency for the incompressible magnetoplasma and the sheathless case, with an electron plasma frequency of 1.0 MHz and electron cyclotron frequency of 1.5 MHz.

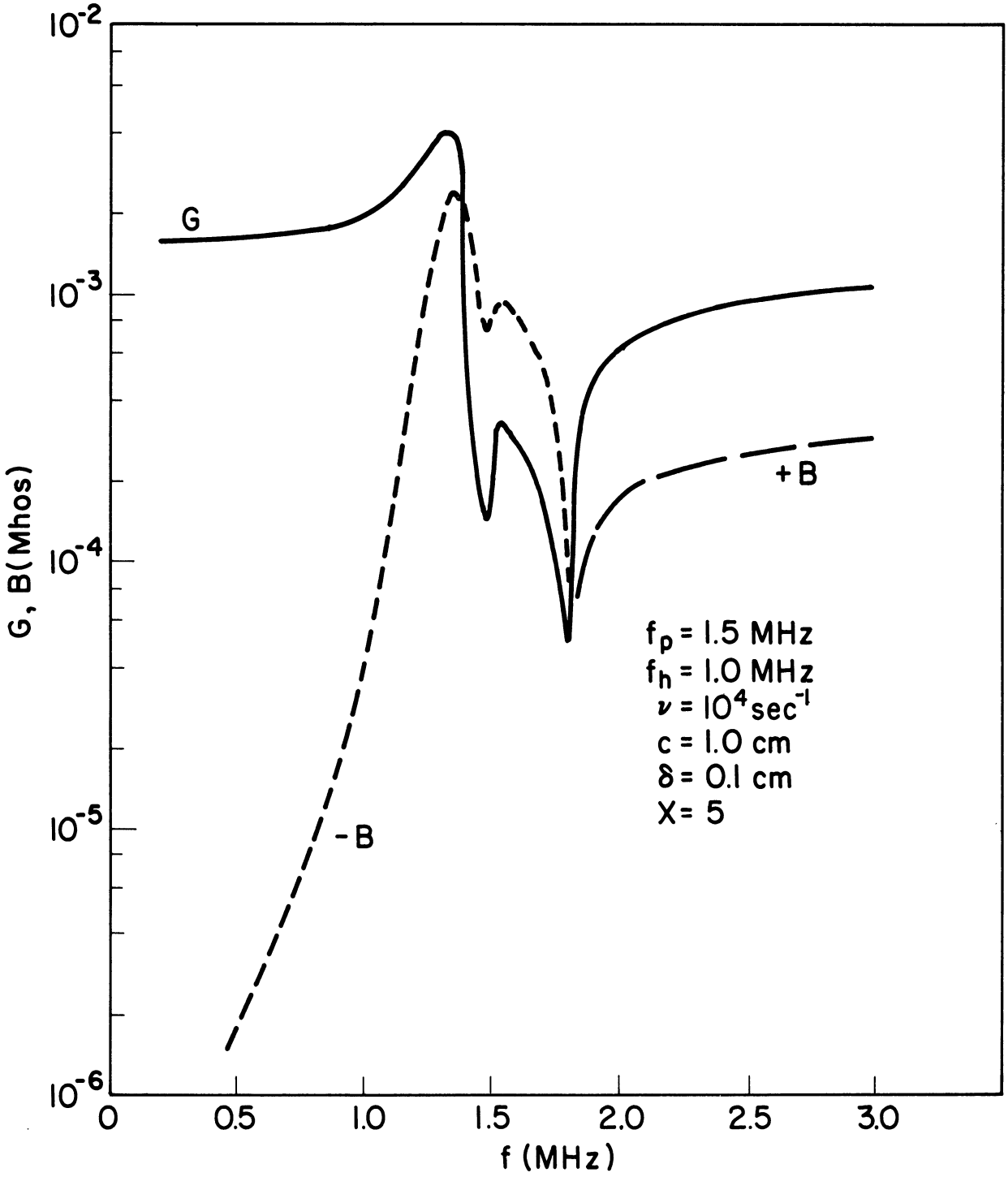

Figure 7. The infinite antenna admittance as a function of frequency in the incompressible magnetoplasma with a vacuum sheath thickness of 5 $D\ell$, an electron plasma frequency of 1.5 MHz and electron cyclotron frequency of 1.0 MHz.

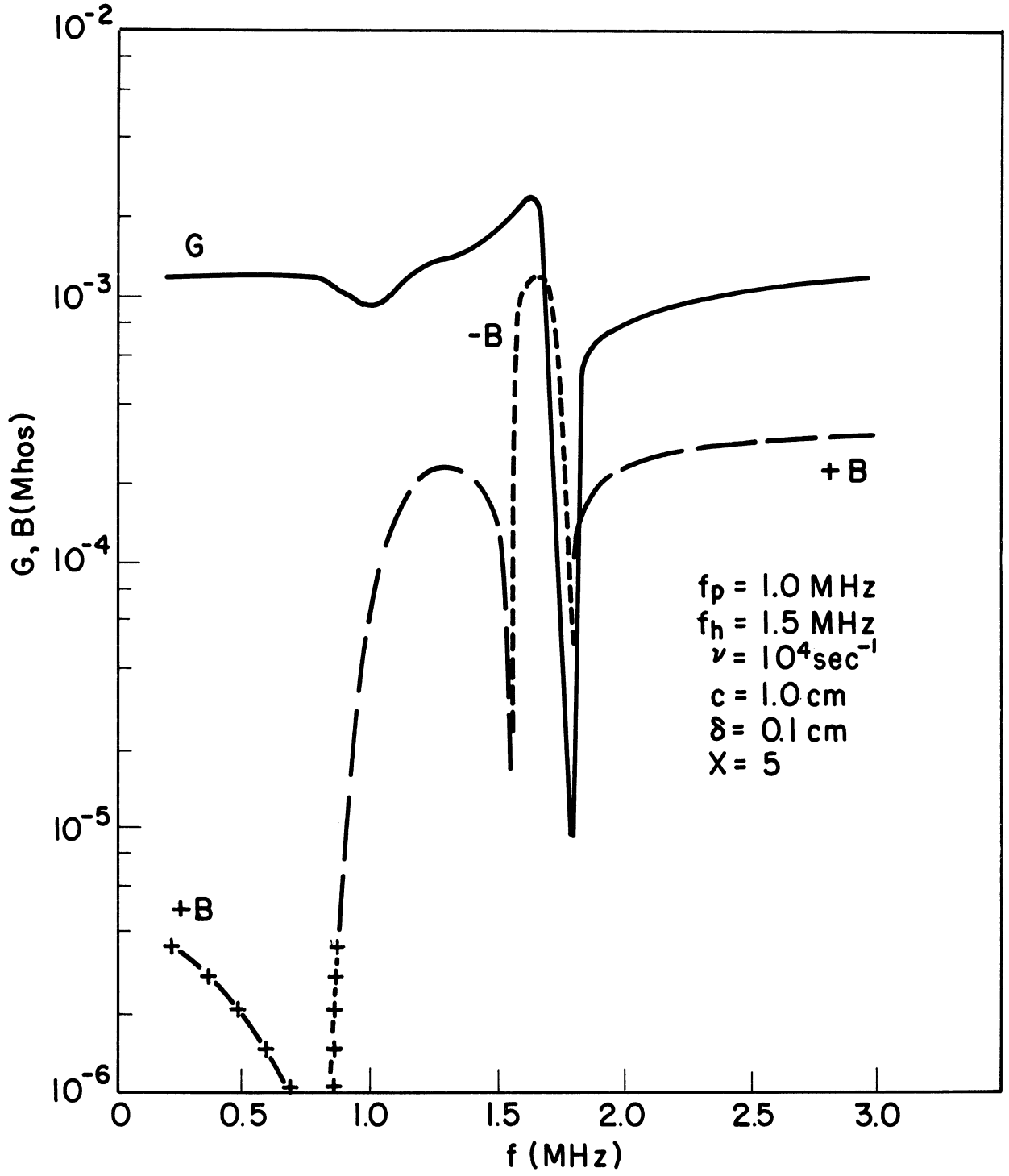

Figure 8. The infinite antenna admittance as a function of frequency in the incompressible magentoplasma with a vacuum sheath thickness of 5 D_ℓ, an electron plasma frequency of 1.0 MHz and electron cyclotron frequency of 1.5 MHz.

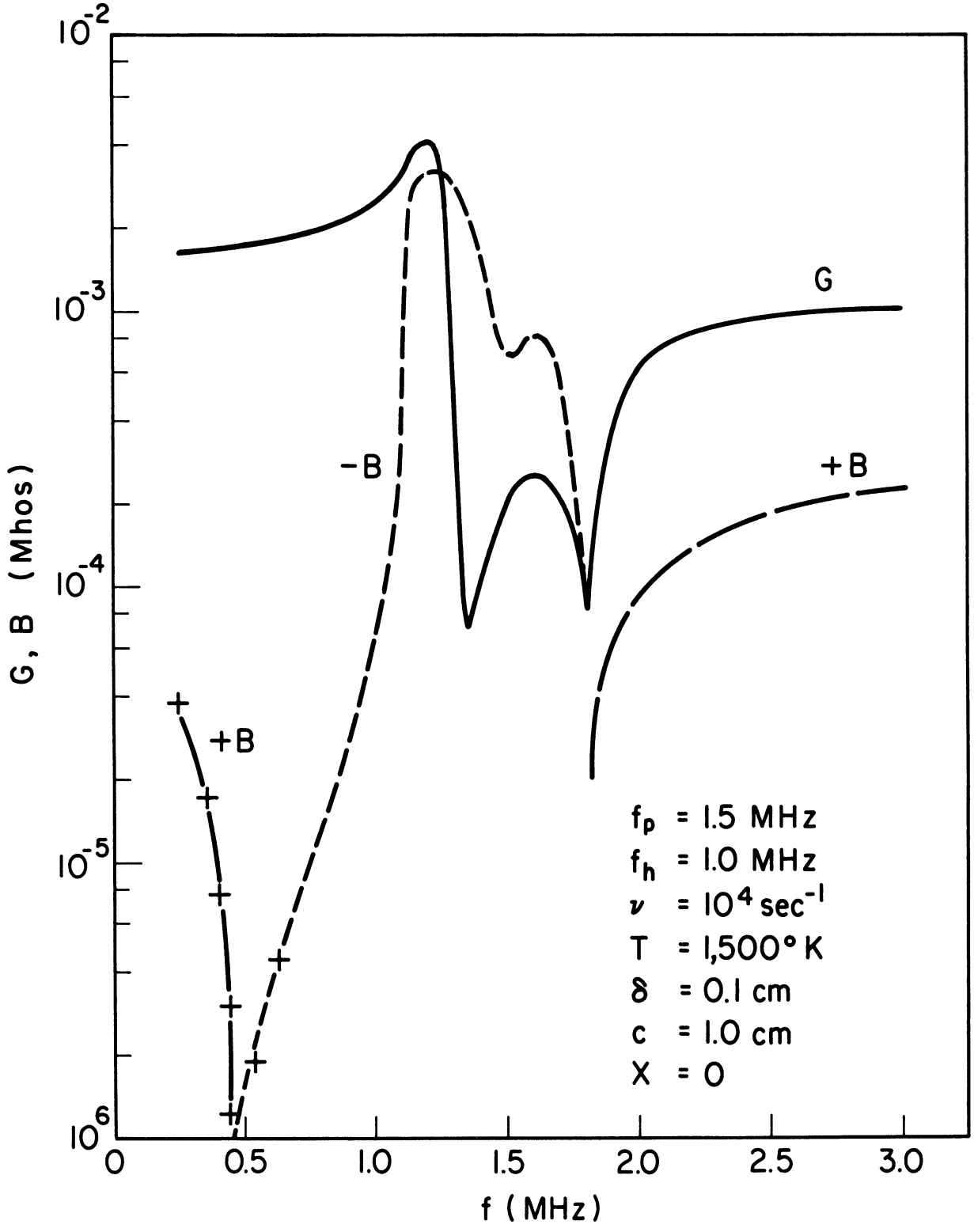

Figure 9. The infinite antenna admittance as a function of frequency for the compressible, magnetoplasma and the sheathless case with an electron plasma frequency of 1.5 MHz and electron cyclotron frequency of 1.0 MHz.

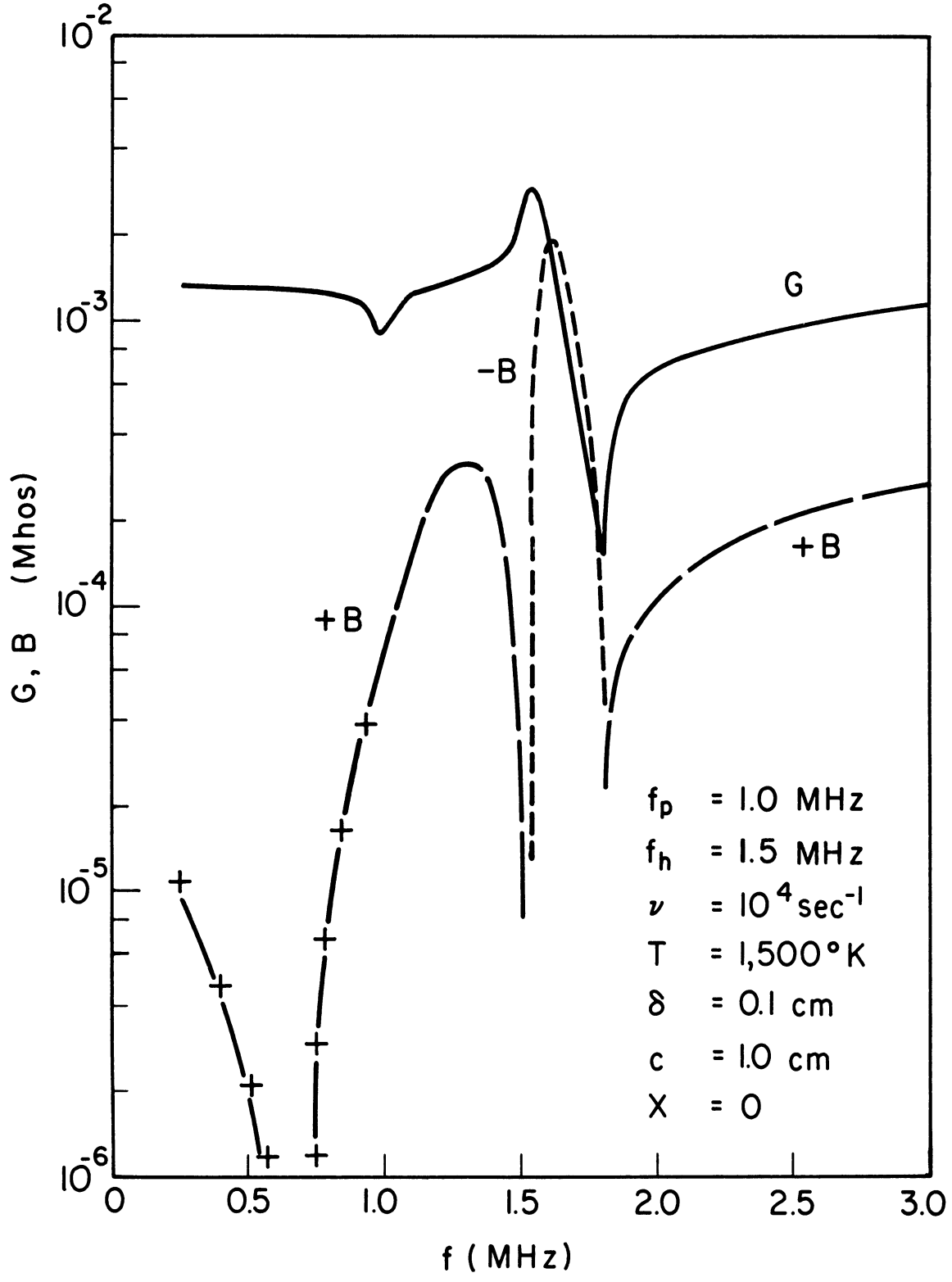

Figure 10. The infinite antenna admittance as a function of frequency for the compressible, magnetoplasma and the sheathless case with an electron plasma frequency of 1.0 MHz and electron cyclotron frequency of 1.5 MHz.

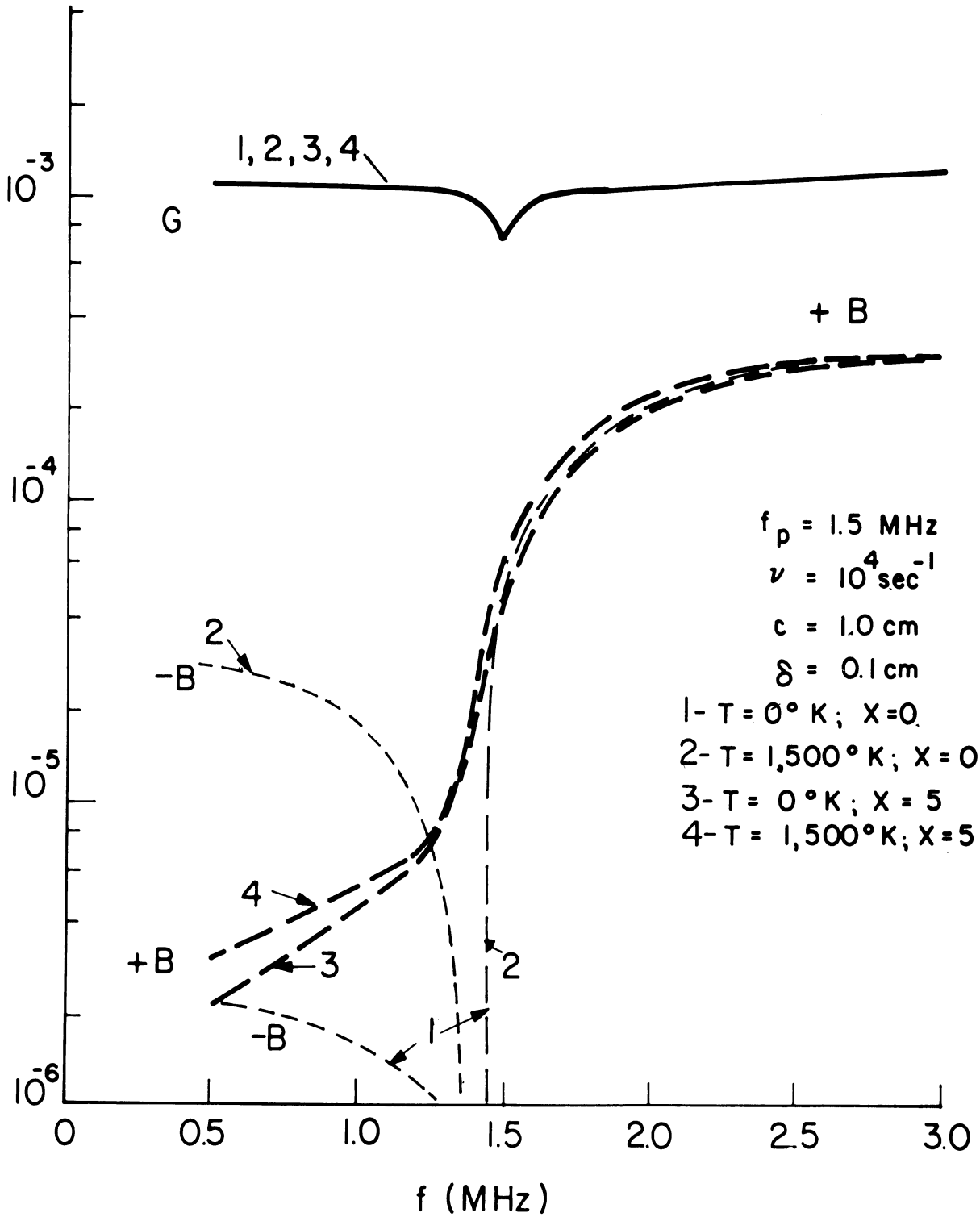

Figure 11. The infinite antenna admittance for the compressible ($T=1500^{o}K$) and incompressible ($T=0^{o}K$) uniaxial plasma for both the sheathless and 5-$D\ell$ vacuum sheath cases.

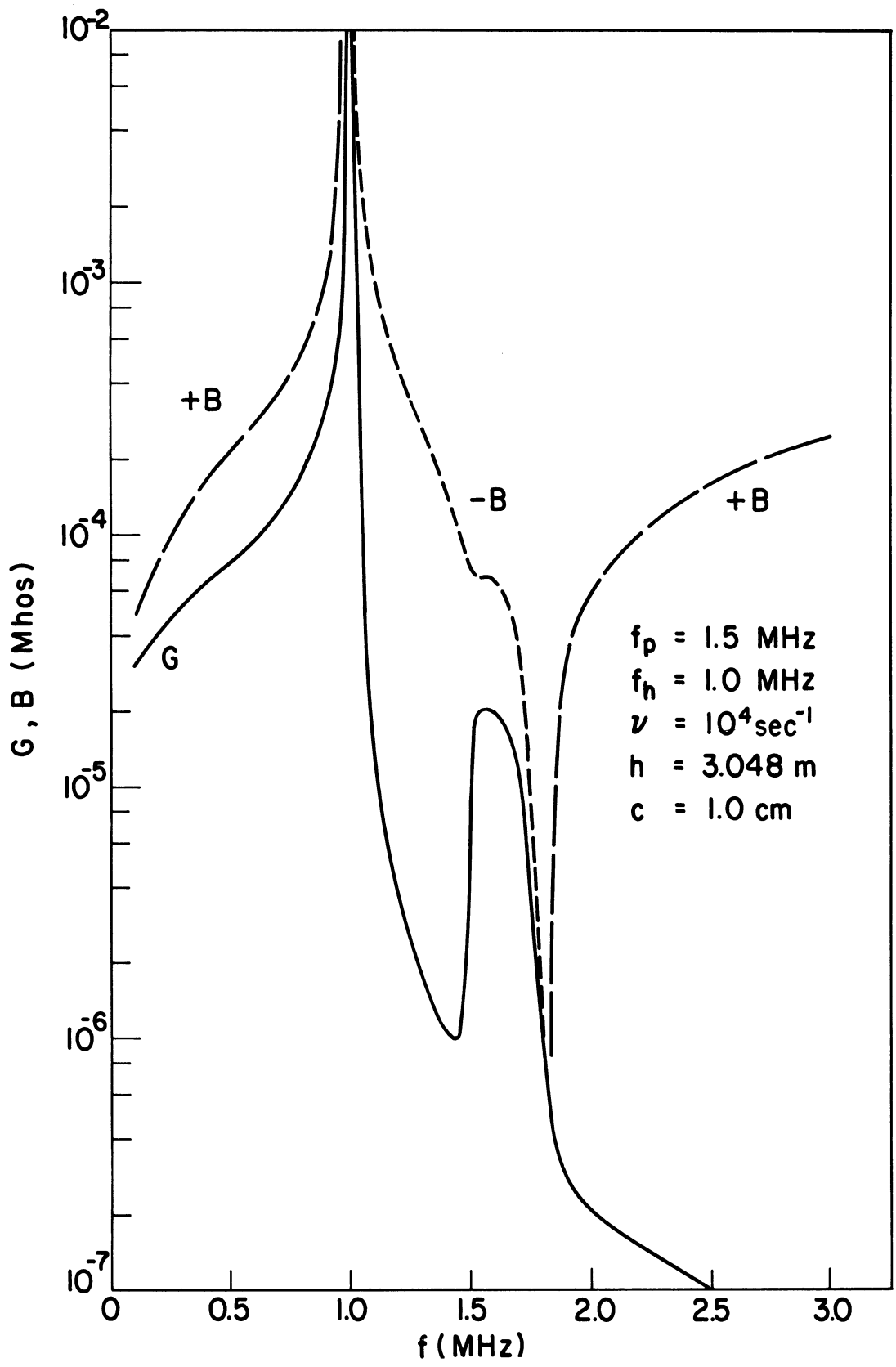

Figure 12. The finite antenna admittance as a function of frequency for the zero-temperature magnetoplasma with an electron plasma frequency of 1.5 MHz and electron cyclotron frequency of 1 MHz from the theory of Balmain (1964).

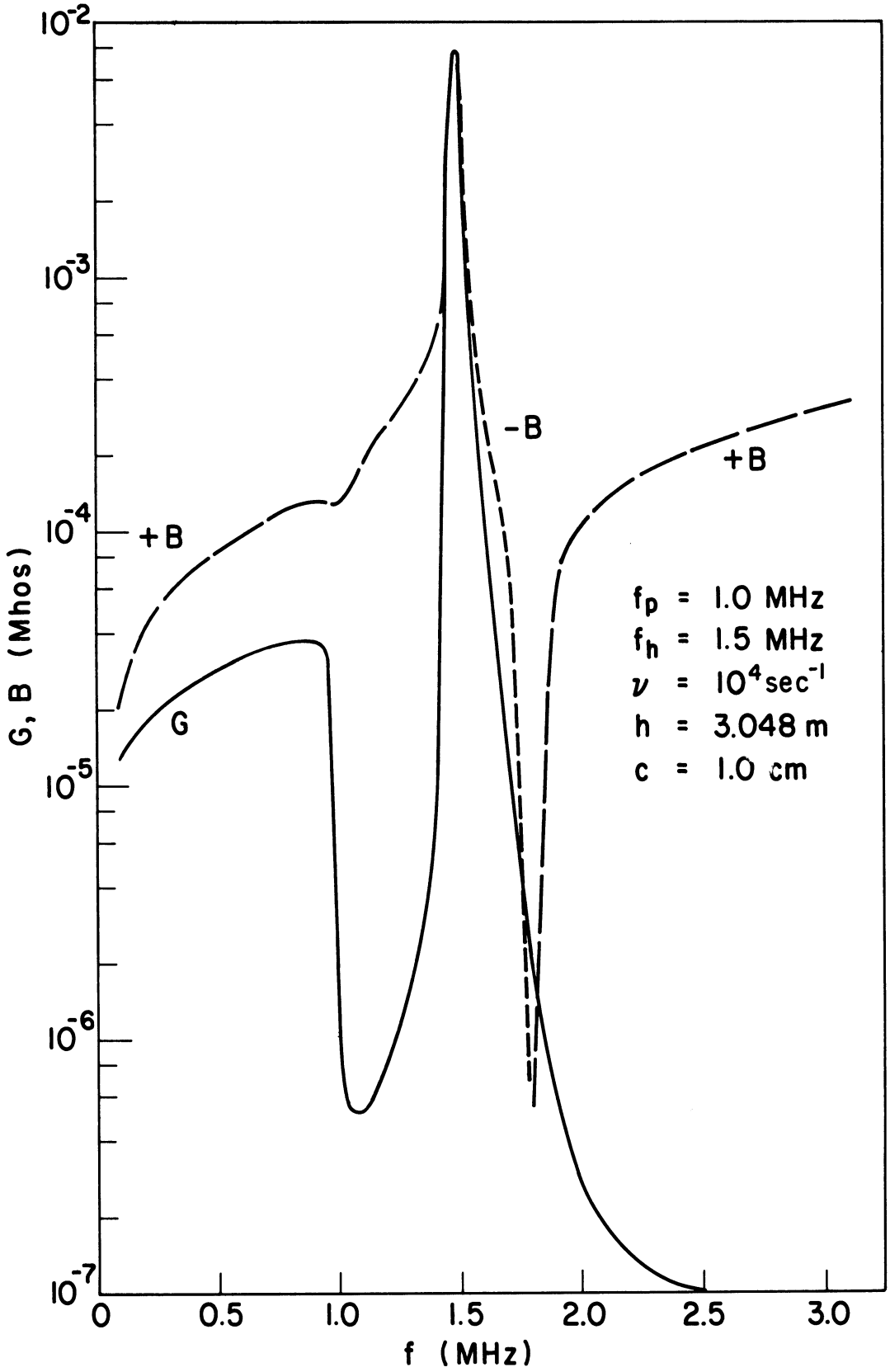

Figure 13. The finite antenna admittance as a function of frequency for the zero-temperature magnetoplasma with an electron plasma frequency of 1 MHz and electron cyclotron frequency of 1.5 MHz from the theory of Balmain (1964).

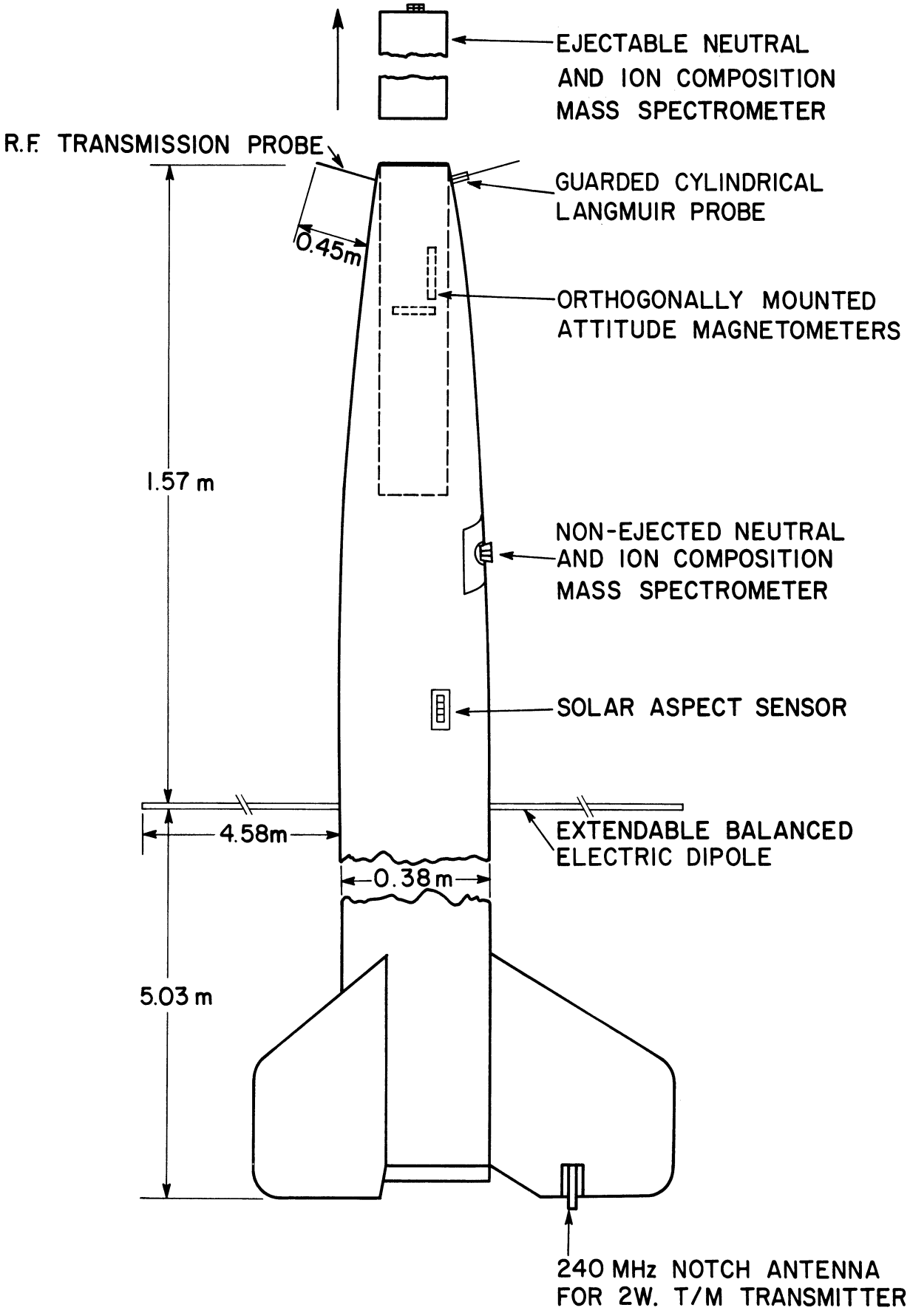

Figure 14. Rocket experiment configuration.

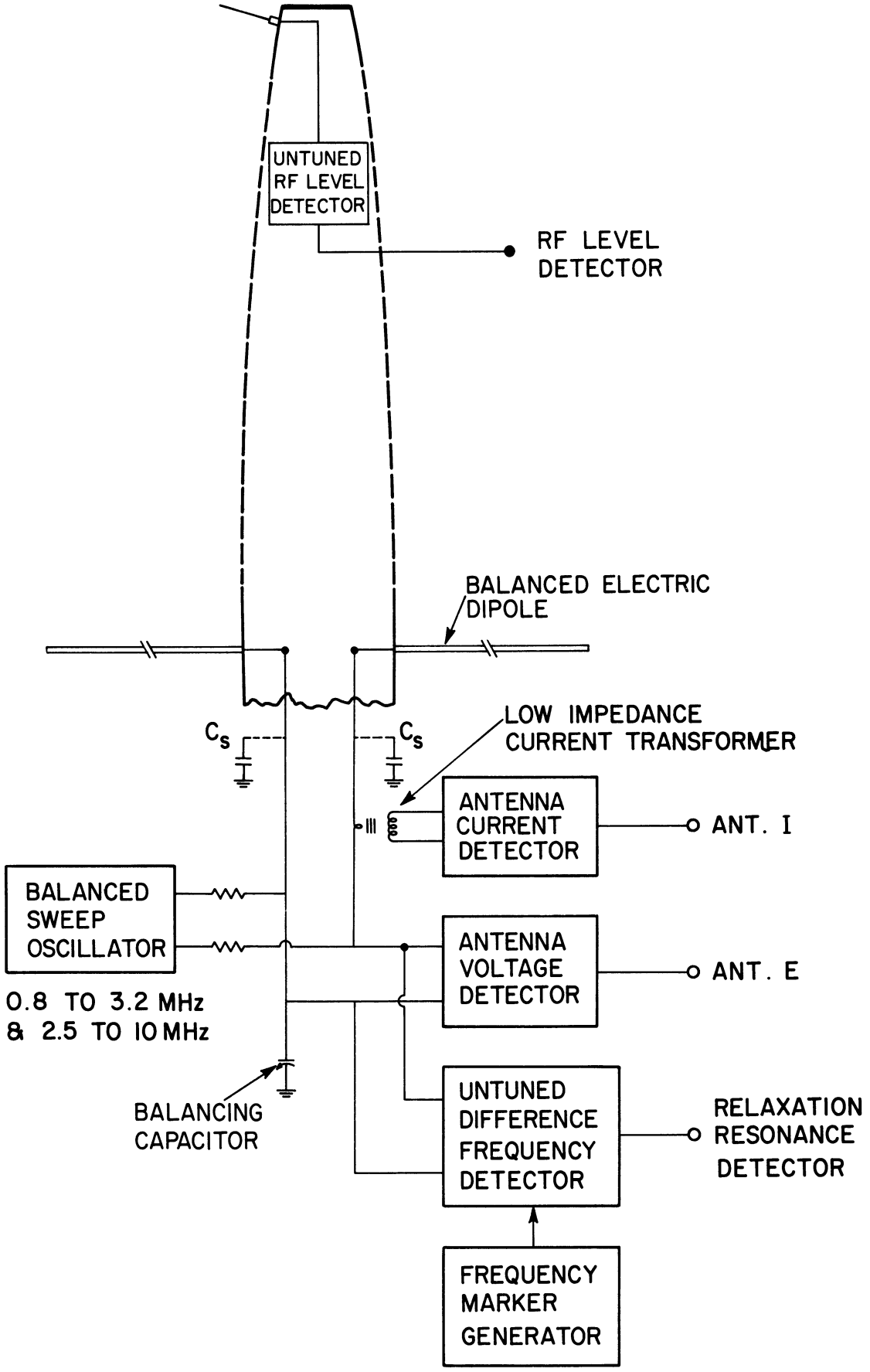

Figure 15. Radio frequency probe schema.

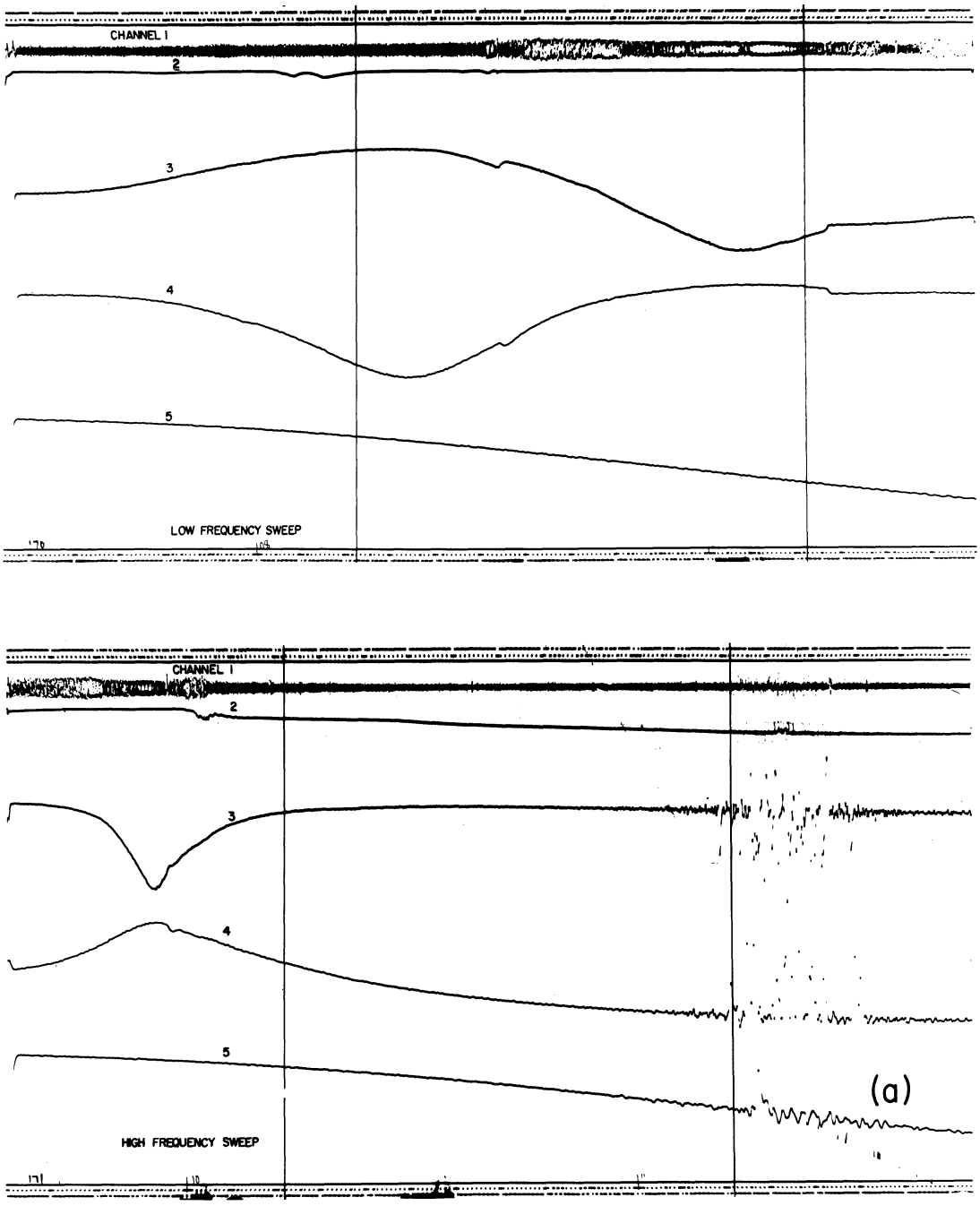

Figure 16. (a) The telemetered data; (b) the experimental half-dipole impedance plotted linear with time; (c) the experimental half-dipole impedance plotted vs. frequency together with the theoretical impedance from Balmain's formula for the plasma medium including the shunt capacitance, and the free-space impedance with and without the shunt capacitance.

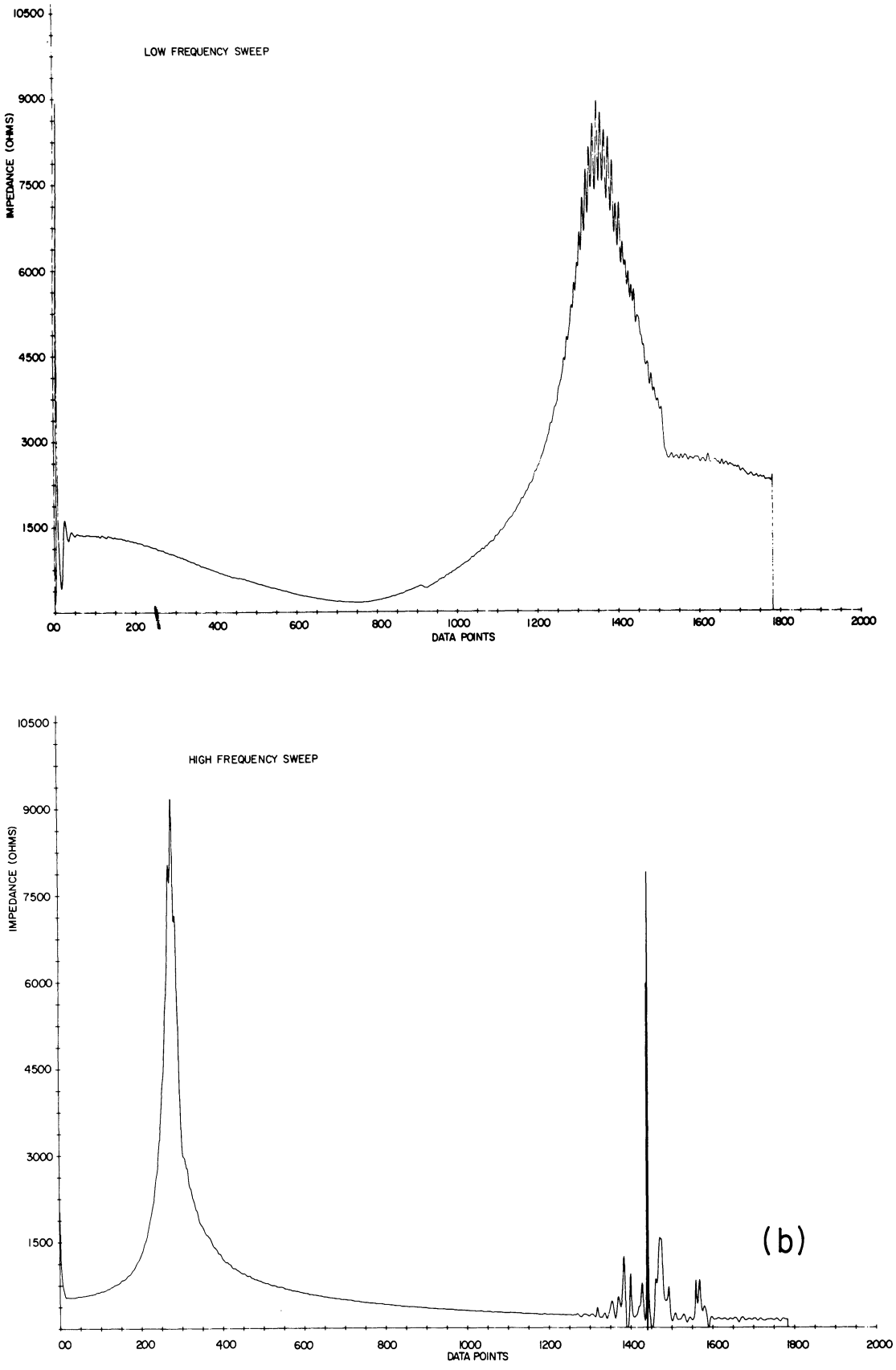

Figure 16. (Continued).

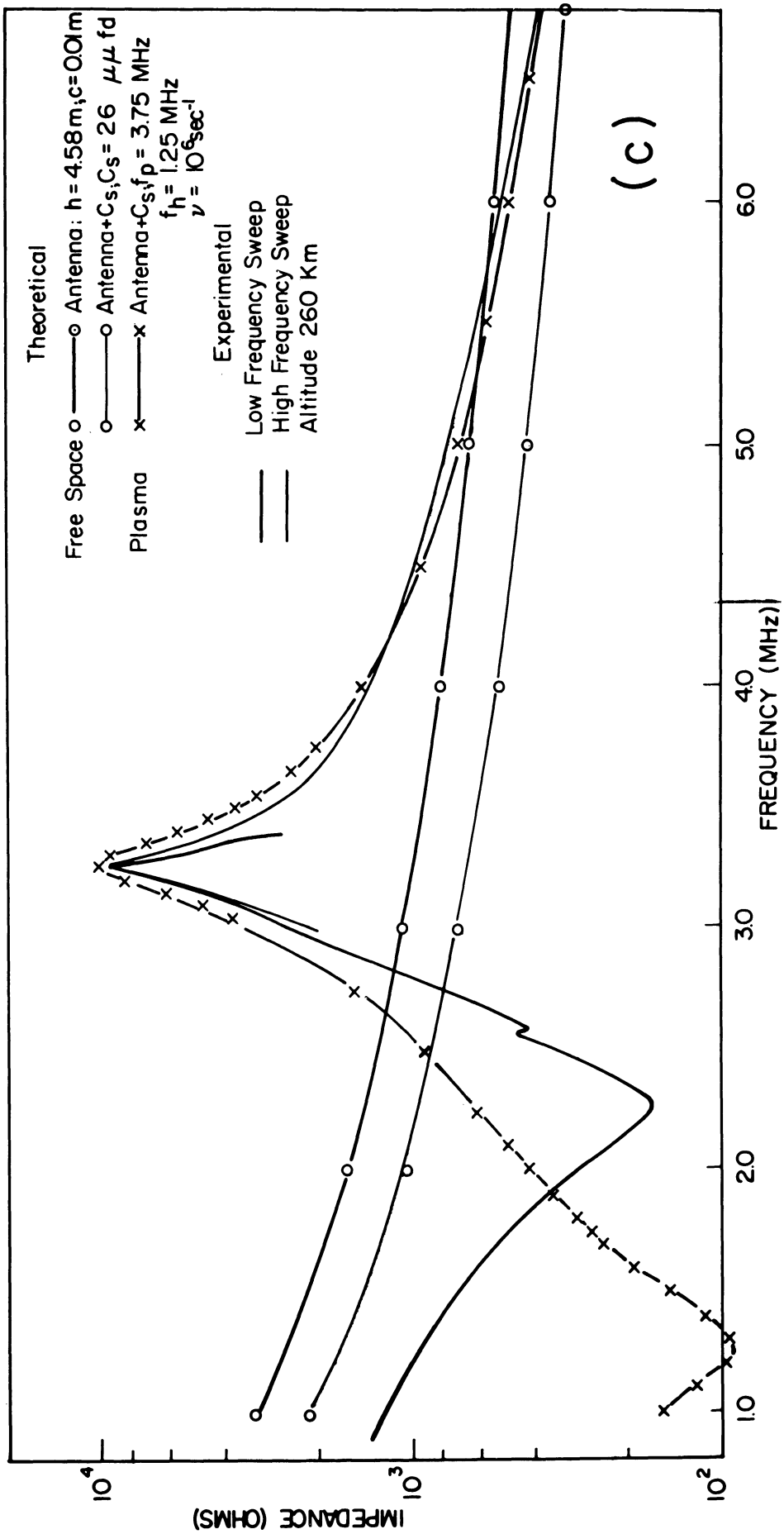

Figure 16. (Concluded).

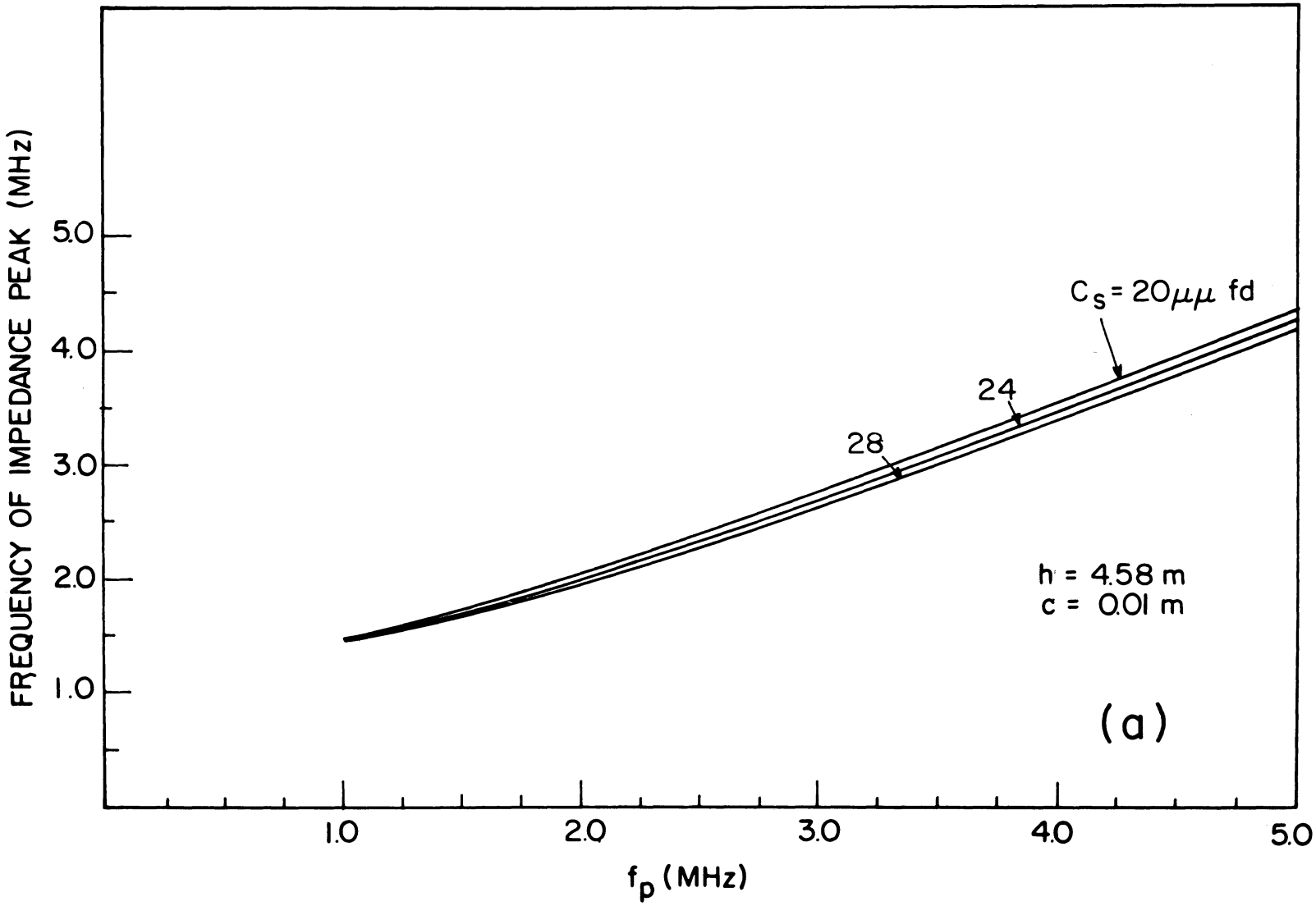

Figure 17. Results calculated for the half-dipole antenna from Balmain's quasistatic impedance formula which show (a) the frequency of the impedance peak and (b) the impedance magnitude at 5.25 MHz as a function of the electron plasma frequency for an electron cyclotron frequency of 1.25 MHz and with the shunt capacitance a parameter.

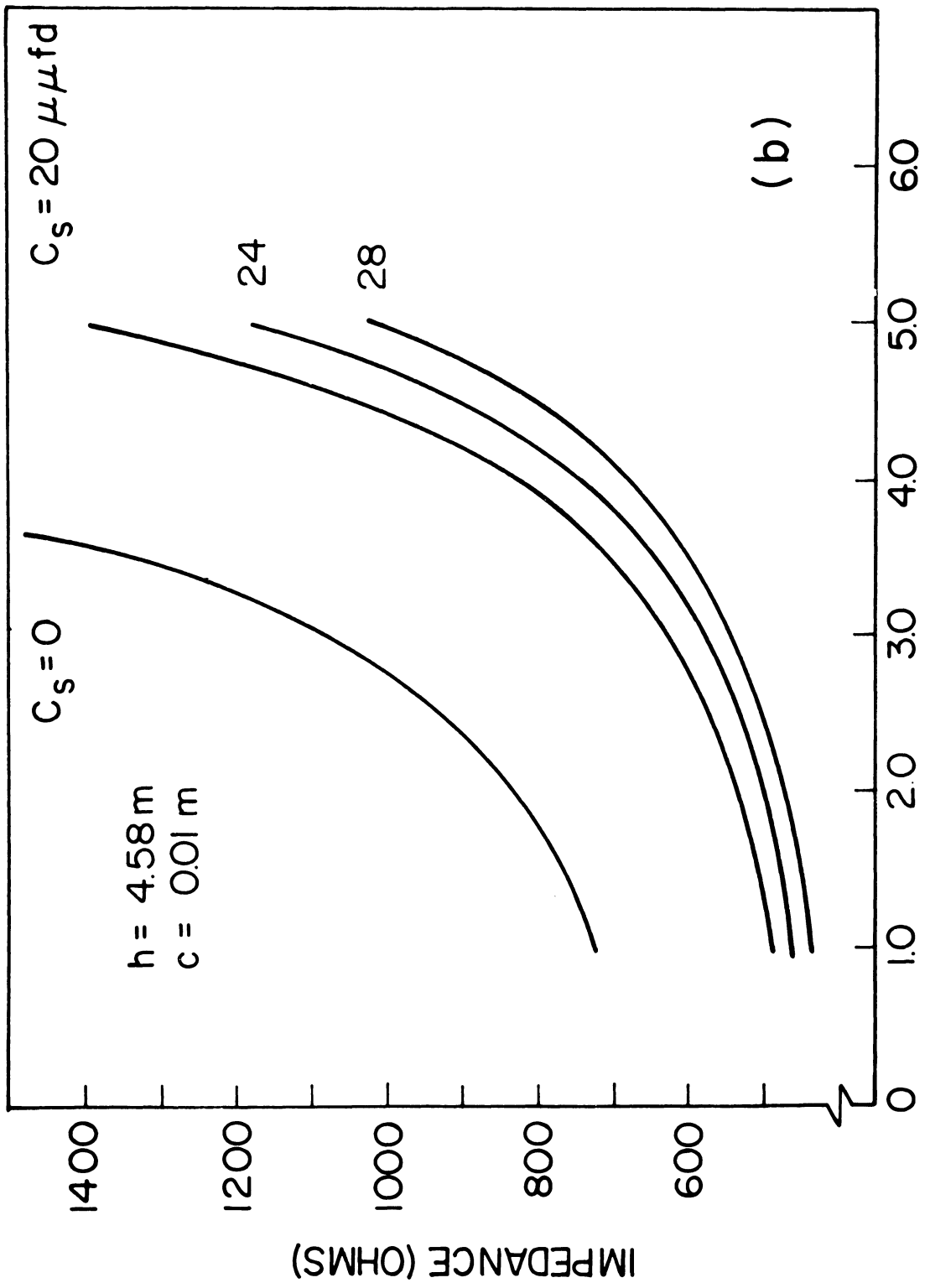

Figure 17. (Concluded).

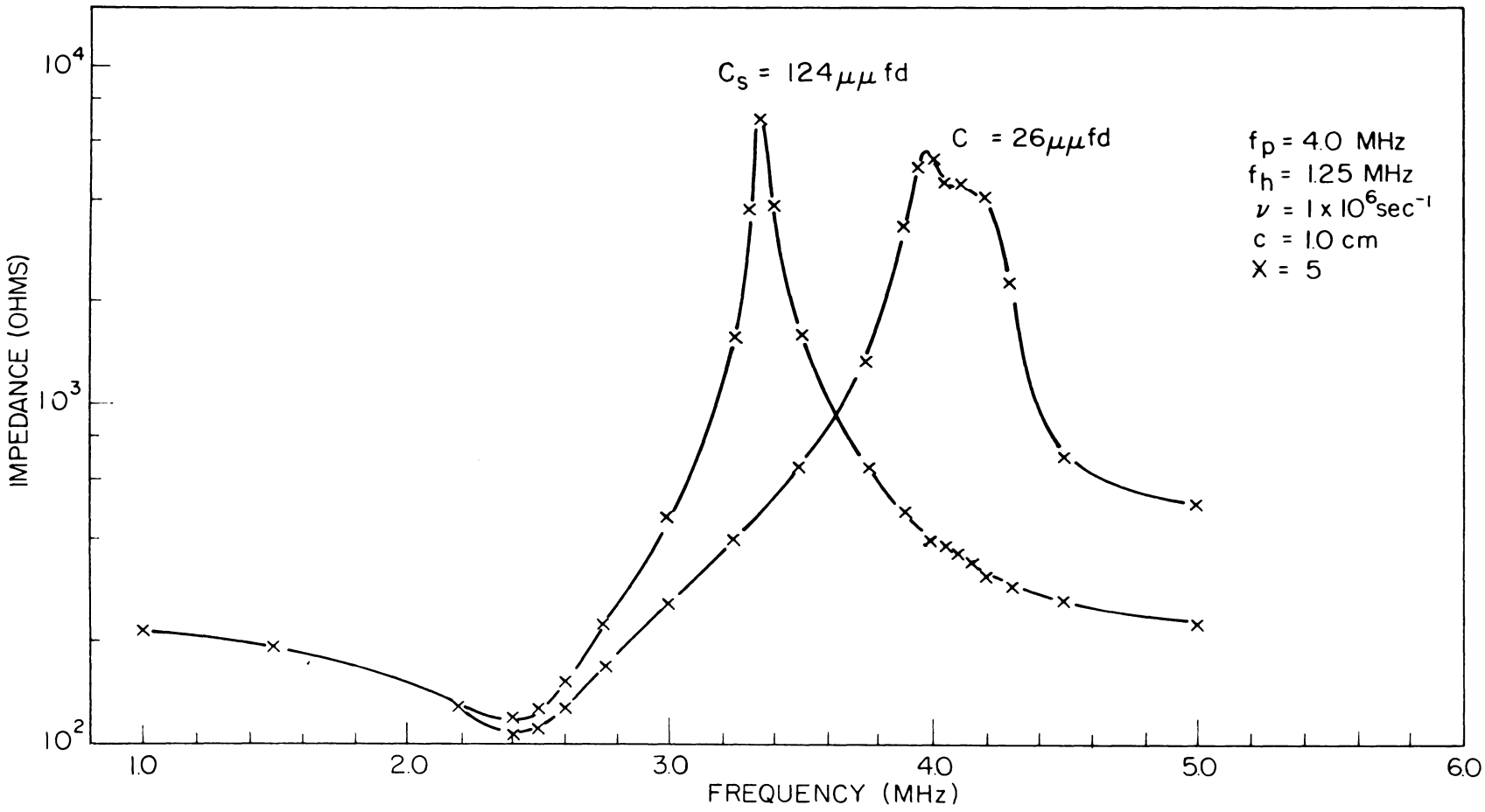

Figure 18. The infinite half-dipole antenna impedance as a function of frequency for the anisotropic, incompressible plasma with an electron plasma frequency of 4.0 MHz, electron cyclotron frequency of 1.25 MHz, and a vacuum sheath 7-Dℓ thick for an electron temperature of 1500°K.

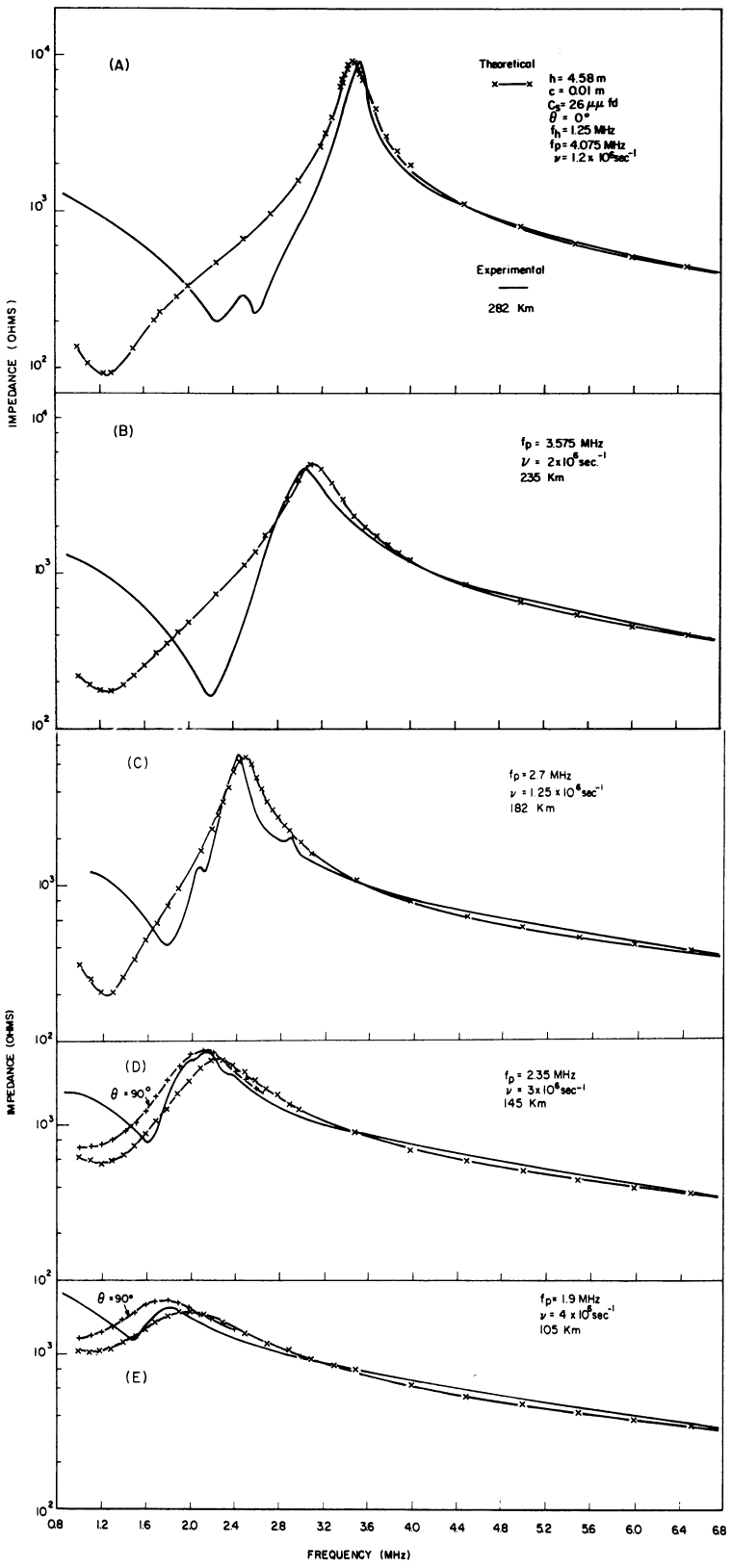

Figure 19. The experimental half-dipole impedance as a function of frequency for several altitudes and the theoretical impedance calculated from Balmain's quasistatic formula for the indicated values of f_p, f_h and ν.

References

Balmain, K. G. (1964), The impedance of a short dipole antenna in a magnetoplasma, IEEE Trans. AP-12, No. 5, 605-617.

Chen, H. C. and D. K. Cheng (1966), Concerning lossy, compressible, magneto-ionic media-general formulation and equation decoupling, IEEE Trans. Ant. Prop. AP-14, 497-501.

Cohen, M. H. (1962), Radiation in a plasma III. Metal boundaries, Phys. Res., Vol. 126, 398-404.

Heikkila, W. J., J. A. Fejer, J. Hughill and W. Calvert (1967), Comparison of ionospheric probe techniques, Proc. VII th Int. Space Sci. Symposium, Vienna, North Holland Publishing Co., Amsterdam.

Mayhan, R. S, and F. U. Schultz (1967), Electromagnetic plane wave scattering from a plasma-coated conducting cylinder, Rad. Sci., Vol. 2, 853-868.

Miller, E. K. (1967 a, b, c,), The admittance of the infinite cylindrical antenna in a lossy plasma: I. The isotropic compressible plasma (Report 05627-10-S): II. The anisotropic incompressible plasma (05627-11-S) : III. The anisotropic, compressible plasma (05627-13-S), U. of Michigan.

Miller, E. K. (1967d), The current and near-fields of an infinite cylindrical antenna in a lossy, plasma medium, U. of Mich. Scientific Report 05627-14-S.